REPORT DOCUMENTATION PAGE

AFRL-SR-BL-TR-00-

0424

maintaining
estions for
ie Office of

1. AGENCY USE ONLY (Leave blank)	2. REPORT DATE	3. REPORT T
	August 3, 2000	Final report, October 1, 1996 - October 1, 1999

4. TITLE AND SUBTITLE
Elevated Temperature Performance of Polymeric Matrix Composites Under Fatigue Stresses in Hygrothermal Environment.

5. FUNDING NUMBERS
AFOSR Grant No.
F49620-97-1-0163

6. AUTHOR(S)
Dr. James C. Seferis

7. PERFORMING ORGANIZATION NAME(S) AND ADDRESS(ES)
Polymeric Composites Laboratory
University of Washington
Benson Hall 243 Box 351750
Seattle, WA 98195-1750

8. PERFORMING ORGANIZATION REPORT NUMBER

9. SPONSORING / MONITORING AGENCY NAME(S) AND ADDRESS(ES)
Dr. Charles Lee
AFOSR/NL
110 Duncan Ave. Suite B115
Bolling AFB, DC 20332-0001

10. SPONSORING / MONITORING AGENCY REPORT NUMBER

11. SUPPLEMENTARY NOTES

12a. DISTRIBUTION / AVAILABILITY STATEMENT
APPROVED FOR PUBLIC RELEASE: DISTRIBUTION UNLIMITED

12b. DISTRIBUTION CODE

13. ABSTRACT *(Maximum 200 Words)*

High performance polymeric composites were investigated for their utilization in more hostile conditions in terms of temperature, humidity, and cycling. A number of commercially available composite systems and model systems developed in the Polymeric Composites Laboratory were selected in this study. The addition of rubber to the cyanate ester matrices was found to reduce the rate of matrix deterioration but caused a substantial increase in water uptake. The addition of a thermoplastic modifier to the cyanate ester matrices increased the thermal stability of the matrices more than the elastomer modifier, however, it did not affect the degradation of the material since degradation was mainly governed by the cyanate ester network. Fiber reinforcement and solvent content of an epoxy matrix composite changed the water absorption rate and mechanical properties of the composite. The changes observed in the hygrothermal cycling studies were examined with the transient simulated laminate methodology using unsymmetric laminates. Finally, a model using equivalent cycle time combined with time-temperature superposition theory was proposed to study long-term properties of composites.

14. SUBJECT TERMS	15. NUMBER OF PAGES
Hygrothermal cycling, environmental effect, composites, cyanate Ester, epoxy.	114
	16. PRICE CODE

17. SECURITY CLASSIFICATION OF REPORT	18. SECURITY CLASSIFICATION OF THIS PAGE	19. SECURITY CLASSIFICATION OF ABSTRACT	20. LIMITATION OF ABSTRACT
Unclas	Unclas	Unclas	

NSN 7540-01-280-5500

Standard Form 298 (Rev. 2-89)
Prescribed by ANSI Std. Z39-18
298-102

ELEVATED TEMPERATURE PERFORMANCE OF POLYMERIC MATRIX COMPOSITES UNDER FATIGUE STRESSES IN HYGROTHERMAL ENVIRONMENTS

AFOSR Final Report

Dr. James C. Seferis
Polymeric Composites Laboratory
University of Washington
Benson Hall 243, Box 351750
Seattle, WA 98195-1750

Submitted to
Dr. Charles Lee
AFOSR/NL
110 Duncan Ave. Suite B115
Bolling AFB, DC 20332-0001

Reference Status: Internal report
PCL Internal No.: 368•8/00•JCS

EXECUTIVE SUMMARY

The most significant advancements and conclusions in this final report can be grouped into three categories: environmental effects on cyanate ester and epoxy composite materials, application of TSL methodology under hygrothermal cycling, and aging analysis through time-temperature equivalence.

Environmental Effects on Cyanate Ester and Epoxy Composite Materials

Low temperature cure cyanate ester resin systems were developed and modified with epoxy-terminated butadiene acrylonitrile rubber (ETBN) and impregnated into woven glass fabric. Mode I and mode II interlaminar fracture toughness values of the cured laminates were evaluated as a function of rubber concentration. Mode I fracture toughness increased to almost twice that of the unmodified system, while mode II fracture toughness remained essentially unchanged. Composite samples were subjected to aging experiments in water and the absorption/desorption behavior and the effect on thermal performance were investigated. The presence of rubber was found to reduce the rate of matrix deterioration but also caused a substantial increase in water uptake. It was found that although the addition of rubber to the matrices decreased the unconditioned (dry) Tg, all specimens showed the same reduction in Tg after equilibrium water absorption.

The effects of temperature and moisture on the thermal and mechanical properties of high temperature cyanate ester composite materials were investigated. A resin transfer molding process was used to impregnate glass fiber fabrics with matrices that underwent thermoplastic or elastomeric toughness modifications. The elastomer-modified material

obtained the highest mode I fracture toughness values primarily because the toughener did not phase separate. Extended exposure to 200 degree Celsius deteriorated initial toughness improvements regardless of the modifier utilized. Although the thermal stability was increased by using thermoplastic modifiers in comparison to the elastomer-modified material, the degradation was mainly governed by the cyanate ester network. Gaseous degradation products caused delaminations and therefore reduced strength when the materials were exposed to 200 degree Celsius for 1000 hours. Also, upon immersion in water at 95 degree Celsius, the matrices absorbed up to 5 weight percent, more than previous values reported in the literature. Fiber/matrix interfacial phenomena were responsible for this behavior because fiber/matrix adhesion was also reduced drastically as shown by the strong reduction in flexural strength.

The effect of fibrous reinforcement and solvent content on moisture uptake in composite laminates was investigated. Two materials using identical epoxy resin systems but different reinforcements - glass vs. carbon fibers - and of different solvent content - low vs. normal - were examined. Samples were characterized in terms of water absorption and desorption. Mechanical and thermal properties including flexural modulus, flexural strength, and glass transition temperature were measured. Results clearly show the contribution of the fiber reinforcement as well as solvent content on the water absorption rate and mechanical property changes.

Application of TSL Methodology Under Hygrothermal Cycling

A non-destructive method was developed to predict the behavior of carbon fiber/epoxy composite materials subjected to hygrothermal conditions. By applying the

transient simulated laminate (TSL) technique, a methodology was developed to evaluate the effects of water ingression on the laminates based on the changes in curvatures. The absorption-desorption-resorption cycle of laminates was evaluated *in situ* by measuring the moisture content and curvatures of unsymmetric laminates $[0_2/90_2]_T$. The laminate curvatures decreased as more water diffused into the laminates until high moisture content was reached. During hygrothermal cycling, the curvature of a laminate was affected by absorption temperature and desorption temperature. This work demonstrated that curvature measurements in addition to moisture measurements could be an effective tool for relating physical state changes to hygrothermal cycling history in composite laminates.

Aging Analysis Through Time-Temperature Equivalence

Composite degradation was investigated by measuring weight loss using quantitative methods. Weight loss experiments were performed on carbon fiber/epoxy laminates under both isothermal and dynamic conditions using various fiber directions and lay-up sequences in the laminate specimens. Weight loss rates were specimen geometry dependent, implying an anisotropic degradation behavior. A model was used to describe the sample weight loss at isothermal temperatures. The model was also used in combination with time-temperature superposition theory to predict the effect of thermal cycling on weight loss to understand the long-term properties of composites. It was found that the model successfully quantified the thermal degradation behavior observed under thermal cycling conditions.

PEOPLE INVOLVED

Principal investigator:

Dr. James C. Seferis	Boeing/Steiner Professor and Director Polymeric Composites Laboratory

Research Fellows:

Dr. Brian Hayes
Dr. Takeshi Takatoya

Research Technologist:

Louise Peterson

Graduate Students:

F. Buehler, R. Hillermeier, J. Klug, J. Shafizadeh, Y.-J. Wu, C. Bruce, S. Guionnet, M. Tillman, F. Chavez, K. Chung

PUBLICATIONS

Buehler, F.U. and J.C. Seferis, Composites: Part A, **31** (7) 741-748 (2000).

Chung, K. and J. C. Seferis, Proc. 43rd Int'l SAMPE Symp., 387 (1998).

Chung, K., J.-D. Nam and J. C. Seferis, Composites Part A, in print (1999).

Hayes, B. S. and J. C. Seferis, Proc. SPE ANTEC 99, New York, (1999).

Hayes, B. S., G. A. Parker and J. C. Seferis, Polym. Eng. and Sci., **40** (6) 1344-1349 (2000).

Hillermeier, R. W. and J. C. Seferis, Proc. SPE ANTEC 99, (1999).

Hillermeier, R. W. and J. C. Seferis, J. of Appl. Poly. Sci., in print (1999).

Nam, J. D. and J. C. Seferis, J. of Poly. Sci., (1998).

Seferis, J. C., J. Composites Technology and Research, July (1999).

Takatoya, T., K. Chung, Y-J. Wu, and J. C. Seferis, Proceedings of ICCM 12, Paris, under Durability and Aging (1999).

Wu, Y.-J., K. Chung, T. Takatoya, C. E. Bruce and J. C. Seferis, Proc. 44th Int'l SAMPE Symp., **44**, 773-781 (1999).

Wu, Y.-J., T. Takatoya, K. Chung and J. C. Seferis, and K. Ahn, J. Composite Materials, accepted (2000).

TABLE OF CONTENTS

INTRODUCTION

High performance polymeric composites have been recognized as attractive engineering materials due to their high strength to weight ratio. However, broadening composite utilization to more hostile conditions in terms of temperature, humidity, and cycling, among others, requires additional stability, especially for the polymeric matrix. The use temperature limitation and the lifetime of polymeric composites are often determined by the polymer matrices because they are less thermally stable than the reinforcing fibers or they actually must protect the reinforcing fibers. When the matrix candidates are chosen for a specific application, evaluation and validation processes should be performed to identify time-temperature relations with the required composite property retention.

The objective of this study was to develop a methodology for characterization and modeling of process, structure, and property relationships in polymeric matrix composites, specifically in those with epoxy and cyanate ester matrices. This work focuses on the stability of these composites when placed in varied temperature, accelerated fatigue stress, and fluid environments. Initially, stability issues were addressed through examination of composite absorption characteristics after cyclic exposure to water at elevated temperature. Following this work was an investigation of microstructural and transitional changes resulting from exposure to water and thermal environments in the form of hygrothermal cycling. Finally, the observed changes with respect to cycling were related using previously developed viscoelastic, time-temperature superposition, and process simulated laminate models.

ENVIRONMENTAL RESPONSE OF ELASTOMER AND THERMOPLASTIC TOUGHENED CYANATE ESTER COMPOSITES

INTRODUCTION AND BACKGROUND

During the last decade, aromatic cyanate esters have emerged as a new class of thermosetting resins for composite matrices in both aerospace and electronic industries. Being derived from cyanation of hydroxyl-containing species, a variety of backbone structures have been studied [1]. These polymers have in turn imparted varying chemical, thermal, mechanical, and dielectric properties. The dicyanate ester monomers cyclotrimerize via addition polymerization to form polycyanurates or triazines [2]. Compared to epoxies and bismaleimides (BMIs), cyanates are considerably more hydrophobic. Cured neat resin specimens only absorb up to 2.5wt% water [1, 3, 4]. Balanced dipoles in the cured state and the absence of hydrogen bonding functionality are responsible for the low moisture absorption and the excellent dielectric properties [5]. The cured network is responsible for high glass transition temperatures (T_g) that are between BMIs and epoxies [5]. Relatively low crosslink densities and high free volumes make cyanate esters inherently tougher than most high temperature thermosets.

These unique features along with their excellent processing characteristics have made cyanate esters desirable for many aerospace applications including radomes, antennae, and low observable structures. However, materials used for these types of applications, as well as others, typically require enhanced performance characteristics that the base resins alone do not possess. Common desires for these materials are increased fracture toughness and improved resistance to micro-cracking. Modifiers such

as elastomers and thermoplastics are usually incorporated into the base resins to improve these characteristics [6]. These materials, however, must be selected so that they do not inhibit processing or reduce other characteristics such as thermal or mechanical performance. As a result, selection of a modifier for a specific material and application becomes increasingly difficult especially when considering long term as well as hot-wet performance.

A variety of modifiers have previously been utilized to improve the toughness performance of cyanate esters. These include reactive and non-reactive elastomers as well as a variety of engineering thermoplastics [7-13]. Most studies, however, considered only neat resin properties which do not always translate directly into composite properties [10, 12, 13]. As a result, the response to toughness modifiers and their implication on processing and durability are not fully understood for cyanate ester composites.

OBJECTIVE AND APPROACH

The objective of this study was to develop an understanding of how high temperature cyanate ester systems can develop additional toughness. In addition, it was of interest to identify how toughness modification influences the processing characteristics and the environmental durability of the resin. To obtain this information a model cyanate ester RTM system was created. The selection of the curing system needed special attention as no data for RTM systems has been published. Two modified systems were established by adding engineering thermoplastics and one system by adding an elastomer. The effects of the modifications on composite processing, morphology, and properties were evaluated. Finally, the materials were subjected to a high temperature environment and to water absorption experiments. The environmental effects on fracture toughness,

mechanical, and thermal properties were analyzed. With this information conclusions could be drawn concerning the impact of modifications on these characteristics and what the dominating factors were.

EXPERIMENTAL

Materials, Model Resin Formulation, and Processing

The base cyanate resin formulation consisted of 50wt% AroCy® B-30 prepolymer, 30wt% AroCy® B-10, and 20wt% AroCy® L-10 monomer supplied by Ciba Polymers. The catalyst for this system was a blend of 2.5 phr nonylphenol and 0.42 phr 2% chromium naphthanate, from OMG America, Inc. Hydroxy functional butadiene acrylonitrile (HTBN) reactive rubber AT x 013 Type III (Echo Resins), polyetherimide (PEI, Ultem® 1000), and polysulfone (PS, Udel® P1800) were used in the amount of 10wt% to toughen the base resin. The finely ground thermoplastics were dried in an vacuum oven for approximately 24 hours at 130°C prior to use. The reinforcement for the laminates was a glass fiber 8 harness satin fabric (style 7781) from Clark-Schwebel Inc. finished in 4354CS-767 cyanate ester tailored sizing.

The base resin was formulated by mixing the cyanate ester monomers and prepolymers at 100°C in an oil bath. After degassing at 80°C the catalyst was added under continuous stirring for three minutes and the material was then quenched to room temperature. The HTBN modified resin was formulated accordingly, except that the elastomer was heated separately before the preheated B-30, B-10, and L-10 resins were added respectively. The PEI and PS modified resins were created by adding the dried, finely ground thermoplastics to the B-10 and L-10 resin mixture under continuous stirring

at 130°C for 3 hours. After adding the B-30 and degassing at 110°C, the resins were cooled to 80°C followed by addition of the catalyst and quenching to room temperature.

0°-symmetric 16 ply laminates with a target fiber volume content of 57% were fabricated using the bleed resin transfer molding (BRTM) process. The materials were cured for 1 hour at 178°C and 2 hours at 240°C using heating/cooling rates of 3.3°C/min and a consolidation pressure of 1 MPa. During the heating to 178°C, two impregnation/consolidation steps (100°C and 115°C) were performed for 15 minutes each to optimize processing.

Environmental Analysis

Cured laminates were cut into 12.7 mm wide specimens and were dried at 110°C for 48 hours (24 hours atmospheric pressure followed by 24 hours vacuum) before they were tested or subjected to thermal aging or water absorption studies. Thermal aging was carried out at 200°C in an air circulation oven. Water conditioning was performed by placing the specimen in a bath that was heated to 95°C and filled with deionized water. The weight of the materials which were subjected to thermal or water conditioning was measured sequentially to monitor weight changes. The coupon sizes were approximately 52 x 12.7 x 3.3 mm (L x W x D) for the thermal aging specimens and 250 x 12.7 x 3.3 (L x W x D) mm for the water absorption experiments.

Testing

The neat resins were analyzed by differential scanning calorimetry (DSC) using a TA Instruments DSC 2910 interfaced to a Thermal Analyst 3100 controller. Dynamic DSC experiments were performed at a heating rate of 5°C/min to 350°C in a nitrogen

atmosphere. The activation energy was determined using heating rates of 2.5°C, 5°C, 10°C, and 20°C per minute (determined using the method by Ozawa and Doyle) [14, 15]. Cure cycle simulations were carried out employing heating/cooling rates of 3.3°C/min. Residual cure analyses were performed by re-heating the cured resins to 350°C at a rate of 5°C/min.

Rheology of the neat resins was investigated using a controlled stress rheometer CSL 100 from TA Instruments. The rheometer was run with parallel plates, an oscillation frequency of 6.28 rad/sec and a heating rate of 2.8°C/min for dynamic experiments.

Mode I interlaminar fracture toughness of cured laminates was measured using the double cantilever beam (DCB) method [16-18]. Specimens were approximately 300 mm long and 12.7 mm wide. A Kapton® film crack initiator, 50.8 mm long, was placed into the midplane during lay-up. The symmetric laminates were laid up so that the warp face of all fabric plies was facing the midplane. Therefore, the fiber tow geometry in the midplane was similar to the geometry obtained by unidirectional materials. Each sample was first pre-cracked in a mechanical testing apparatus to provide a sharp crack tip before the test was performed. For all materials at least five specimens were tested. Samples were pulled apart at a rate of 25.4 mm/min until a final displacement of 63.5 mm was observed.

Mode II interlaminar fracture toughness was measured using the end-notch flexure (ENF) test [17, 18]. The laminates were prepared in the same manner as the DCB specimens. A three-point bending apparatus with stationary posts set at 76.2 mm apart was used to create shear fracture in the midplane of each specimen. The crack tip was set

19.05 mm from the stationary post and the loading point was set 38.1 mm in the midpoint of both posts. Specimens were pre-cracked in the mechanical testing apparatus to provide a sharp crack tip before testing was performed. A displacement rate of 2.54 mm/min was used to load the specimen in flexure until the load decreased upon crack propagation.

Flexural properties were determined in a three-point test according to ASTM D790 [19]. For each material, five specimens with a length of 60 mm and 12.7 mm width were tested. The support span was 48 mm and the cross-head speed was 1.2 mm/min. To determine the temperature dependent viscoelastic properties, dynamic mechanical analysis (DMA) was carried out on cured materials with a TA Instruments DMA 2980 using single cantilever clamps. A heating rate of 5°C/min in conjunction with a oscillation frequency of 1 Hz was utilized.

Morphology of the cross sections of cured laminates was examined by optical microscopy. The HTBN modified material was stained with osmium tetroxide while the PEI and PS modified materials were etched with methylene chloride and MEK, respectively.

Fracture surfaces were also investigated using optical and scanning electron microscopy (SEM). The SEM analysis was performed using an accelerating voltage of 25 kV and a working distance of 20 mm.

RESULTS AND DISCUSSION

Resin Characteristics

The base model resin containing cyanate monomers and prepolymers was formulated so that RTM adequate characteristics were obtained. The bisphenol A dicyanate monomer (AroCy® B-10) and prepolymer (AroCy® B-30) were the main ingredients. The utilized ratio provided satisfactory rheological characteristics, which are necessary for low viscosity impregnations. However, these two resins tended to crystallize at ambient temperatures due to the symmetry of the bisphenol A dicyanate monomer (BADCy). Hence, liquid dicyanate monomer AroCy® L-10 was incorporated into the formulation as it provided resistance against crystallization of the overall formulation due to its asymmetric molecular structure [1, 20]. Although the formulation still tended to crystallize after a relatively long time at the ambient temperature, the resin exhibited satisfactory transition points. Rheometry showed that the four systems exhibited viscosities quite different from each other (Figure 1). The unmodified resin reached a minimum viscosity of approximately 2×10^{-3} Pa•s at 120°C which is adequate for RTM processing [21].

The modification by HTBN increased the viscosity only a small degree due to the low molecular weight of the elastomer. Thus, this HTBN modified resin was also suitable for conventional RTM. However, the addition of PEI and PS to the cyanate ester formulation increased the viscosity significantly and resulted in resins that were too viscous for conventional RTM processing. Consequently, the bleed resin transfer molding technique was employed to process highly modified resin systems in a RTM like manner [8, 9].

In RTM processing the selection of the catalyst is important because the resins typically need to maintain low viscosity values for longer periods to provide enough time for impregnation. Catalysts that are latent but still result in high conversions must be employed. Chromium napthenate in conjunction with nonylphenol has been previously found to offer these features [8, 9]. Differential scanning calorimetry (DSC) revealed that the activation energy for the catalyzed formulation was 77.5 kJ/mol. The catalyst lowered the reaction onset of the uncatalyzed resin from approximately 200°C to 130°C. This provided enough latency for sufficient laminate impregnation for BRTM processing. Isothermal rheometer experiments at 100°C and 120°C confirmed that the viscosity did not change significantly over 30 minutes.

The heat of reaction for the modified resins was around 550 J/g, approximately 10% lower than the observed heat of reaction for the unmodified system. This difference in heat of reaction corresponded to the weight fractions of modifiers in these three systems. The measured exotherm peak temperatures were approximately 5°C higher for the systems containing PEI and HTBN, suggesting that these modifiers might have hindered to a small extent the trimerization reaction of the cyanate ester groups. The addition of polysulfone, however, increased the peak temperature slightly. This shows that this system may have reacted differently than the other two materials.

The optimum processing conditions were defined using the DSC cure cycle experiments. In this study it was desirable to obtain complete conversion for the following aging experiments. However, this has been a controversial issue since optimum properties are sometimes obtained below 100% conversion [7]. Good results were obtained when the materials were cured for 2 hours at 240°C. The conversion was

> 99% and the associated glass transition temperatures were 266°C, which are in the range of the values reported in literature for similar cyanate ester systems [1, 3, 22].

Properties of Unconditioned Laminate Materials

The cured laminates had fiber volume contents of 57% +/- 1.5% which were determined by using the laminate thickness, material densities, and the assumption of void free laminates.

The mode I interlaminar fracture toughness was measured to investigate the effect of the modifiers on the damage resistance of the cured laminates. Mode I interlaminar fracture toughness was calculated as G_{IC}, the critical energy release rate, which was defined by the area method [16, 17]. The developed composite systems reached toughness values higher than found for most toughened epoxy composite systems (Table 1) [6, 23]. This was partly a function of the cyanate ester chemistries which are known to reach toughness values greater than those obtained by most highly crosslinked matrices [7]. Another important factor for the relatively high toughness values was the glass fibers which exhibit high strain-to-failure values (up to 5%). The G_{IC} values were found to increase by approximately 20% when either the HTBN elastomer or the PEI was included in the base formulation(Table 1). These were relatively small improvements compared to the values found in literature for neat resin properties [10, 24]. However, resin properties often do not translate directly into composite properties and greater improvements are commonly found using higher modifier concentrations [24]. In addition, the four matrices were primarily developed to serve as high temperature materials which were more stable due to the complete conversions.

The results of the mode II interlaminar fracture tests showed similar trends and were in the range between 1 and 1.3 kJ/m^2. However, the test results for each material are not reported here as fiber bridging in the interlayer occurred to a large extent. Therefore, the measured values might represent fiber dominated situations and not the true interlaminar properties. SEM analysis of the fracture surfaces showed that fibers were pulled out of the matrix (Figure 2). As can be seen from the figure the stresses applied in mode II caused the matrix to crack, which again caused the fibers to delaminate.

The fibers probably possessed strain-to-failure values greater than the brittle matrix, therefore, they remained intact in some cases causing fiber bridging between the two fracture surfaces.

The high conversions found by DSC were confirmed by DMA experiments, which showed that the base material had a glass transition temperature (T_g) of 271°C, as defined by the peak in the loss modulus (Table 1). The T_g values decreased by 20°C for the HTBN and 5°C for the PEI modified system. This suggested that the HTBN and PEI modifiers did not phase separate to a great extent in the cured systems. The PS modified system, however, maintained the T_g of the unmodified system indicating that a high degree of phase separation occurred. It is likely that for the same reason the mode I interlaminar fracture toughness was not improved for the PS modified system, which can be seen in Table 1. As has been reported previously, highly crosslinked matrices with a tough second phase rarely lead to sufficient increases in mode I fracture toughness [25-27].

Optical microscopy of polished cross-sections revealed that all four materials were well impregnated and essentially void free. It was found that a second phase was

formed in the PS modified cyanate ester (Figure 3) confirming the DMA findings. The observed domain sizes were between 2 and 20 μm. The HTBN modified materials did not contain a second phase, however, the PEI modified system showed phase separation to a small extent.

While the mode I and mode II interlaminar fracture toughness results identified the toughness performance, the three-point bend tests characterized the flexural moduli and strengths of the developed composite systems. These are crucial to consider as toughness improvements usually lead to sacrifices in the modulus of the material. The flexural moduli were calculated using the linear section between 25% and 75% of the maximum load of the load-displacement plot, the results of which are depicted in Table 1. Surprisingly, the flexural moduli were not affected significantly by the addition of the modifiers, although the HTBN and PEI materials must have plasticized the matrix to some extent. This was probably partially due to the fact that cyanate esters can reach their maximum modulus when the crosslink density is below the maximum value [7]. In addition, it is important to notice that the moduli in the flexural mode are greatly dominated by the reinforcing fibers. The measured flexural strengths followed the same trend as the flexural moduli (Table 1). All four systems had similar strength levels indicating that structural integrity was not affected by the addition of the modifiers.

Thermal Degradation and Property Response

In aerospace industries the maximum allowable usage temperature for polymeric composite materials is usually defined to be at least 50°C below the temperature where the storage modulus starts to decrease drastically. This point was obtained for all four

cured cyanate ester materials at approximately 250°C, therefore, 200°C was selected as the aging temperature to simulate realistic peak temperature aging conditions.

The results of the weight measurements are shown in Figure 4. As shown in the figure, all materials lost less than 0.5% weight during the 1200 hours at 200°C.

The majority of the gaseous products evolving from the four materials are believed to be based on degradation products of the cyanate ester. Shimp et al. reported that at temperatures ≥ 200°C polycyanurates outgas notable amounts of CO_2 from carbamates, which are formed when residual cyanate functionality encounters moisture in air at temperatures producing segmental mobility [3, 28]. They observed a weight loss of 2% when dicyanate ester castings (BADCy) were exposed to 235°C for 500 hours. Although the cyanate ester network was the major contributor to the measured weight loss, variations among the differently modified systems could be identified. The HTBN modified material lost substantially more weight than the other three materials during this period, possibly a result of the degradation of the butadiene acrylonitrile rubber. Interestingly, the thermoplastic modified systems were the most stable, loosing on average between 15 - 20 % less than the control (Figure 4). This was more than the weight fractions of the thermoplastics contained in the composites. It seemed likely that the thermoplastic portions of the matrices improved the thermal stability of these system, possibly due to entanglement between the crosslinked cyanate ester network.

The effect of toughness modifications on morphology, thermal, and mechanical properties has been studied for a large variety of cyanate ester materials [8-10, 24]. Nevertheless, the effect of high temperature environmental exposure on the toughness properties has not been investigated for cyanate ester composites. Figure 5 compares the

mode I interlaminar fracture toughness values obtained for the unaged materials and the same materials subjected to thermal aging at 200°C for 500 hours. As can be seen from the figure, the exposure to high temperatures had detrimental effects on the toughness performance of all four materials. Degradation of the matrix as well as fiber/matrix interface might have led to the decay of the material properties. Interestingly, the toughness improvement for the unaged materials obtained through the incorporation of the HTBN or PEI was completely deteriorated. These two materials including the control showed the same mode I value after the thermal aging experiment.

It appeared that the degradation of the toughness properties was governed by the degradation of the cyanate ester network. SEM analysis confirmed these findings. Figure 6 shows the fracture surface of the HTBN modified material.

As seen from the figure, intensive hackling took place in resin rich areas indicating relatively brittle fracture. These fracture characteristics were found for all materials. In addition, large areas of delaminated fibers were observed. The relatively small decrease in mode I toughness for the PS modified system suggested that the second phase helped to retain the toughness when the continuous phase lost its ability to absorb stresses induced by the propagating crack tip.

The flexural properties were measured after 500 and 1000 hours of thermal aging in air at 200°C. The flexural strength was found to decrease only by 5 - 7 % when the materials were aged for 500 hours (Figure 7). Matrix embrittlement and possibly fiber/matrix interfacial phenomena may have caused the decay. A trend among the different materials was not observed suggesting that weakening was caused mainly through aging of the cyanate ester network.

Microscopy of the specimens demonstrated that the materials did not microcrack or delaminate. After 1000 hours, however, the strength values were found to decay by approximately 20 % for the unmodified and the HTBN modified systems. As found by microscopy, the surface plies started to delamimate, probably due to formation of volatile products during the degradation of the matrix. This "swelling" phenomenon has been observed previously by other researchers and was believed to be the limiting degradation mechanism in long term service at high temperatures [28, 29]. It could be concluded that the majority of the strength decrease was caused by the swelling of the specimens. For the thermoplastic modified systems, delamination of the surface plies occurred to a smaller extent if at all. This helped the thermoplastic modified materials to retain approximately 90% of their initial flexural strength. The results of the weight analysis are in good agreement with these findings as it was found that the thermoplastic modified materials were the most thermally stable systems. Similar observations are represented in Figure 8 where flexural moduli for the different materials are depicted. After 500 hours of aging time, the composite moduli increased by approximately 5% for all materials, possibly caused by matrix embrittlement. After 1000 hours, however, the materials behaved quite differently. The moduli declined for the unmodified and HTBN modified material, mainly a result of the delaminated surface plies.

The moduli of the PEI and PS modified materials increased slightly confirming that fewer areas were delaminated and additional matrix embrittlement took place. Dynamic mechanical analysis of the aged specimens was carried out after 500 and 1200 hours in the high temperature environment. It was found that after thermal aging for 500 hours the glass transition temperatures remained in the same range for all materials

except for the HTBN modified cyanate ester (Figure 9). This verified that the increase in stiffness of the cyanate ester laminates was not gained through post cure effects, but through embrittlement of the matrix.

The HTBN modified system, however, showed transitions at 199°C and 246°C, possibly a result of a partially degraded cyanate ester network. Also, the degradation of the HTBN, as found by the weight analysis (Figure 3), might have been responsible for this phenomenon. The plot of the relative storage modulus E' for the base and the HTBN modified cyanate ester laminates in their initial and aged version reinforces this assumption (Figure 10). As can be seen from the figure, the temperature dependence of the modulus increased substantially when the HTBN modified material was exposed to thermal aging. It is evident that this particular material loses its high temperature properties to a greater extent than the unmodified cyanate ester material after being exposed to high temperatures. The PEI and PS modified cyanate esters were found to retain the temperature dependent storage modulus in a manner similar to the base system.

Interestingly, the materials behaved quite differently after they were exposed to 200°C for 1200 hours. Figure 11 depicts a plot of the relative loss moduli for the four materials. Unlike the unaged materials, all four materials exhibited two transitions indicated by the peaks in the loss moduli. The first transition was, with the exception of the HTBN modified system, at approximately 195°C. The second transition was in the range of the transitions of the unaged materials. This behavior suggested that localized degraded areas in the cyanate ester existed in the thermally aged material. Although a few studies have focused on the degradation of cyanate esters [3, 22, 28], such behavior has not been reported in the literature. Nevertheless, the results are in agreement with the

findings of the mechanical tests and the microscopy results. As shown before, changes in laminate structure due to outgassing led to a significant reduction in the mechanical performance between 500 and 1000 hours of aging. Although it was assumed that the evolving gas was CO_2 (as shown by other researchers), this should not have led to chemical degradation of the cyanate ester network [1, 3]. Therefore, it was believed that chain scission took place to a significant extent so that localized degraded areas existed in the cyanate ester networks.

Water Absorption and Property Response

Cyanate esters are known to exhibit excellent hot-wet properties because they absorb less water at saturation than competing resins such as epoxies or BMIs. This is mainly a result of the cyanurate linkage which is very resistant to hydrolysis [22]. The key aspect to success in avoiding the deleterious effects of moisture for cyanate esters and epoxies is complete conversion. The hydrolysis of a cyanate function leads to a carbamate which can decompose above 190°C [30]. Shimp et al., however, found that hydrolysis takes place very slowly and suggested that moisture might be absorbed mainly through physical absorption [31, 32].

The results of the water absorption experiments are shown in Figure 12. All composite materials exhibited similar behavior and the total amount of water absorbed after 500 hours in 95°C water was between 0.82 wt% and 0.88 wt%. This water gain approximately corresponded to the 5% weight gain of the cyanate ester matrix assuming that water was only absorbed by the matrix and not by the fibers. Shimp et al., however, observed only 2% water absorption for a similar resin system after 500 hours immersion in boiling water. It is believed that the fibers in the material contributed to the different

behavior. The sizing material might have affected the matrix stoichiometry close to the matrix/fiber interface leading to changes in hydrophobicity or interfacial phenomena such as wicking. The small differences among the four materials were possibly a result of slightly different resin contents of the analyzed specimens.

Mode I interlaminar fracture toughness results for the water conditioned specimens are shown together with unconditioned and thermally aged specimen in Figure 5. As one can see from the figure, the wet mode I toughness performance increased slightly for most materials partly because plasticization of the matrix occurred. SEM analysis, however, indicated that poor interfacial adhesion was apparent as many ruptured fiber bundles with no resin residues were found on the fracture surfaces (Figure 13). Although no discrepancies were observed during mode I testing, the large amount of delaminated fibers might have caused fiber bridging during testing.Fiber bridging usually leads to increases in the interlaminar fracture toughness as parts of the stresses in the interlaminar zone are carried by the fibers [33, 34]. Hence, the observed values have to be read with caution.

The flexural properties were measured after immersion in water for 500 hours. As expected, the flexural modulus decreased for all materials (Figure 14). Matrix plasticization due to water absorption can account for such behavior. Trends among the four materials were not obvious, suggesting that the materials were equally plasticized as already indicated by the weight analysis. The modifier did not seem to have a great influence on absorption behavior, partly because of their small weight contributions to the overall formulations. Hence, the moduli were affected similarly. The flexural

strength was affected more significantly than the flexural modulus for the four systems as shown in Figure 15.

After water immersion, these materials lost about 50% of their initial strength. Again poor interfacial adhesion was possibly the reason for the large decrease. The interfacial adhesion, commonly a function of the fiber sizing, has been shown by many researchers to effect flexural and interlaminar strength values [35, 36].

Dynamic mechanical analysis confirmed that large amounts of water were absorbed by all materials. The glass transition temperatures (T_g) declined to approximately 160°C for all materials as shown in Figure 16. This is in good agreement with the findings of Shimp et al. for a resin system containing only B-30 [1]. As the T_g's for the conditioned materials were in the same range, it could be concluded that the modifiers did change the hydrophobicity of the matrices as already indicated by the weight analysis.

CONCLUSIONS

In the present work, a model cyanate ester resin for high temperature applications was developed. By establishing a catalyst system that provided latency and using a certain resin composition the obtained model matrix had adequate RTM characteristics. Once the base RTM system was developed, three toughened versions, which were modified with 10wt% of either an elastomer or thermoplastic, were formulated. After impregnation of these resins into glass fiber fabric using the BRTM process, the effects of the modifiers were characterized in relation to fracture toughness, flexural, and thermal properties. Essential to this analysis was further comparison of these properties to the properties after thermal aging at 200°C in air and conditioning at 95°C in water. It was

initially found that only modifiers that did not phase separate during cure (polyetherimide and HTBN) led to improvements in the mode I interlaminar fracture toughness. In contrast, polysulfone was found to phase separate and caused no improvements in the mode I fracture toughness.

After subjection to thermal aging for 500 hours, the toughening effects were deteriorated. Primarily matrix embrittlement of the cyanate ester network was responsible for these losses. Further thermal aging at 200°C caused reductions of up to 20% in strength after 1000 hours. Gaseous degradation products evolving from the matrices were assumed responsible for such behavior as they caused delamination. Dynamic mechanical analysis confirmed that the HTBN modified material was most susceptible to degradation and indicated that localized degraded areas in the cyanate ester existed in all four materials.

The water absorption behavior of the four composite systems was not affected by the type of modifiers used. Thus, all materials responded similarly after immersion for 500 hours at 95°C. Surprisingly, the four matrices absorbed more water than typically observed for neat resin specimens. This phenomenon was believed to be due to fiber sizing and interfacial phenomena. Great reductions in flexural strength, up to 50%, after immersion in water for 500 hours demonstrated that the fiber/matrix interface was affected. Matrix plasticization and increased fiber bridging, however, led to slightly increased mode I fracture toughness values.

This work demonstrated that toughness improvements for high temperature cyanate ester systems can be obtained using polymeric modifiers that do not phase separate. The information gained from the environmental studies identified the

degradation mechanism and the influencing factors relative to the modification. Collectively, this knowledge can be used to develop toughened cyanate ester based RTM composite systems for environmentally demanding applications.

REFERENCES

1. Shimp, D.A., Christenson, J.R., and Ising, S.J., 34th Int. SAMPE Symp. Exhib., 222 (1989).

2. Bauer, M. and Bauer, J., Chemistry and Technology of Cyanate Ester Resins, I. Hamerton edt., Blackie Academic and Professional, Glasgow, UK (1994).

3. Ising, S.J., Crawley, Z.F., and Merriman, G.L., 5th Int. SAMPE Electronics Conf., 286 (1991).

4. Speak, S.C., Sitt, H., and Fuse, R.H., 36th Int. SAMPE Symp., 336 (1991).

5. Mackenzie, P.D. and Malhotra, V., Chemistry and Technology of Cyanate Ester Resins, I. Hamerton edt., Blackie Academic and Professional, Glasgow, UK (1994).

6. Hayes, B.S., Simulation Engineering of Polymeric Prepreg Composite Systems, Doctorate Thesis, University of Washington (1997).

7. Hamerton, I., Chemistry and Technology of Cyanate Ester Resins, Blackie Academic & Professional, London, UK (1994).

8. Hillermeier, R.W., Hayes, B.S., and Seferis, J.C., 26th NATAS Conference, Cleveland, OH, 99-104 (1998).

9. Hillermeier, R.W., Hayes, B.S., and Seferis, J.C., Polymer Composites, **20** (1) 155 (1999).

10. Hwang, J.W., Park, S.D., Cho, K., Kim, J.K., Park, C.E., and Oh, T.S., Polymer, **38** (8) 1835-1843 (1997).

11. Zeng, S., Hoisington, M., and Seferis, J.C., 37th Int'l SAMPE Symp., 348 (1992).

12. Srinivasan, S.A. and McGrath, J.E., Appl. Polym. Sci., **64** 167-178 (1997).

13. Borrajo, J., Riccardi, C.C., Williams, R.J.J., Cao, Z.Q., and P., P.J., Polymer, **36** (18) 3541-3547 (1995).

14. Ozawa, T., Journal of Thermal Analysis, **2** 301-324 (1970).

15. Doyle, C.D., Journal of Applied Polymer Science, **5** (15) 285-292 (1961).

16. Whitney, J.M., Browning, C.E., and Hoodgsteden, W., Journal of Reinforced Plastics and Composites, **1** 297 (1982).

17. Pagano, N.J. 'edt.', Interlaminar Response of Composite Materials, **5**, Elsevier, New York (1989).

18. Putnam, J.W., Composite Prepreg Process Characteristics, Doctorate Thesis, University of Washington (1996).

19. Standard Test Method for Flexural Properties of Unreinforced and Reinforced Plastics and Electrical Insulating Materials, ASTM D 790M - 93, (1993).

20. Ciba, R., AroCy L-10 Cyanate Ester Monomer, (1996).

21. Brent Strong, A., Fundamentals of Composites Manufacturing, C.A. Ploskonka, SME, Dearborn, MI (1989).

22. Hamerton, I., Chemistry and Technology of Cyanate Ester Resins, I. Hamerton edt., Blackie Academic & Professional, (1994).

23. Hayes, B.S. and Seferis, J.C., Polymer Engineering and Science, **32** (2) 257 (1998).

24. Srinivasan, S.A. and McGrath, J.E., High Perform. Polym., **5** 259-274 (1993).

25. Hillermeier, R.H., Hayes, B.S., and Seferis, J.C., 44th Int. SAMPE Symp. and Exhib., Long Beach, CA, (1999).

26. Zeng, S., Hoisington, M., and Seferis, J.C., Polymer Engineering and Science, **14** (6) 458 (1992).

27. Shaw, S.J., in Rubber Toughened Engineering Plastics, A.A. Collyer edt., Chapman and Hall, London (1994).

28. Shimp, D.A., 32nd Int. SAMPE Symp., 1063 (1987).

29. Chung, K. and Seferis, J.C., 43rd Int. SAMPE Symp., Anaheim, CA, (1998).

30. Pascault, J.P., Galy, J., and Mechin, F., Chemistry and Technology of Cyanate Ester Resins, I. Hamerton edt., Blackie Academic & Professional, Glasgow, UK (1994).

31. Shimp, D.A. and Ising, S.J., Am. Chem. Soc. National Meeting PMSE Division, San Francisco, CA, (1992).

32. Shimp, D.A. and Chin, B., Chemistry and Technology of Cyanate Ester Resins, I. Hamerton edt., Blackie Academic and Professional, Glasgow (1994).

33. Briscoe, B.J. and Williams, D.R., Composite Science and Technology, **46** (3) 277-286 (1993).

34. Chai, H., International Journal of Fracture, **43** (2) 117-131 (1990).

35. Drzal, L.T. and Madhukar, M., Journal of Material Science, **28** 569 (1993).

36. Stuart, M. and Alstadt, V., 21st Int. SAMPE Technical Conference, 264 (1989).

Table 1 Properties of unaged glass fiber reinforced cyanate ester composites.

	CE	CE + HTBN	CE + PEI	CE + PS
Interlam. Fract. Toughness G_{IC} (J/m²)	557 ± 64	669 ± 12	653 ± 74	563 ± 36
Flexural Modulus* (MPa)	23100 ± 188	23530 ± 133	23183 ± 230	23594 ± 211
Flexural Strength* (MPa)	674 ± 14	661 ± 4	691 ± 15	667 ± 6
Tg by Peak in E''(°C)	271	251	265	272

(± values correspond to standard deviations for at least four measurements, * flexural properties were linearly normalized to 57% fiber volume content)

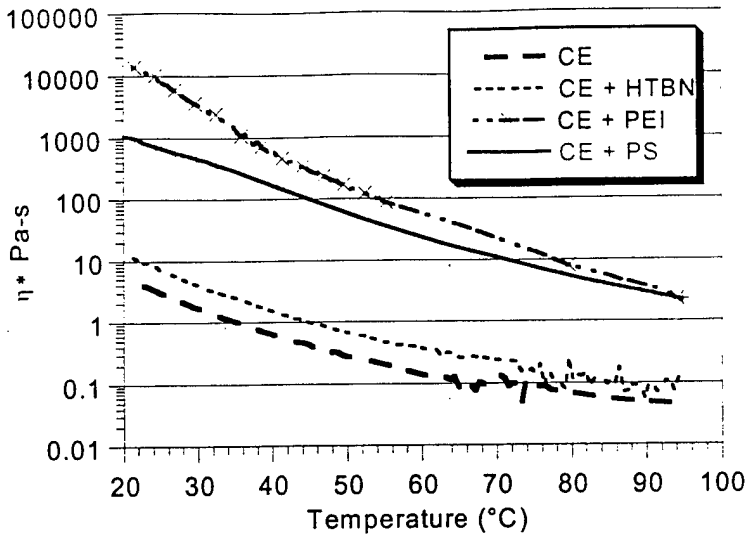

Figure 1 Complex viscosities of four model cyanate ester (CE) resins containing different modifiers (heating rate: 2.8°C/min).

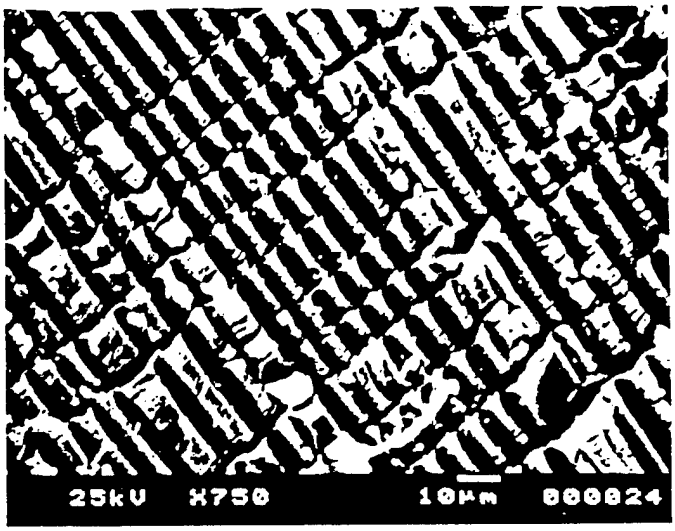

Figure 2 SEM micrograph showing mode II fracture surface of HTBN modified cyanate ester composite material. Grooves caused by delaminated fibers and low strain-to-failure behavior of matrix (cracks)

Figure 3 Cross-section of PS modified cyanate ester material showing PS domains (dark areas) in resin rich interlayer.

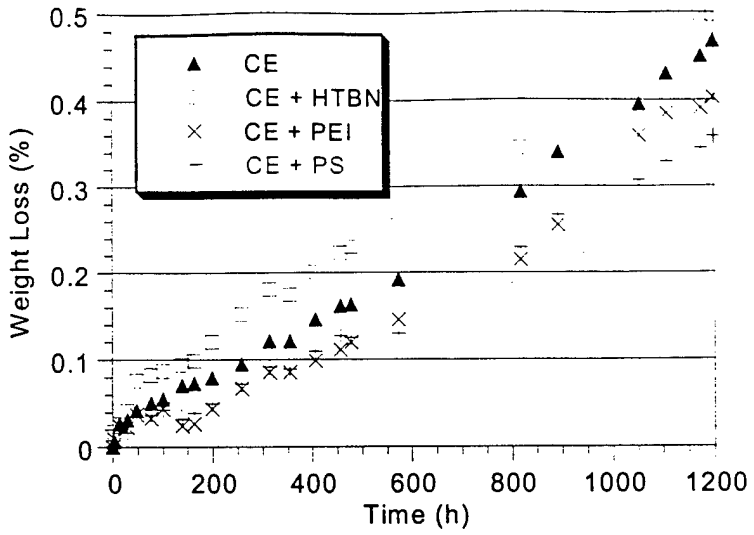

Figure 4 Weight loss caused by thermal aging in air at 200°C of four model cyanate ester (CE) composite systems containing different modifiers.

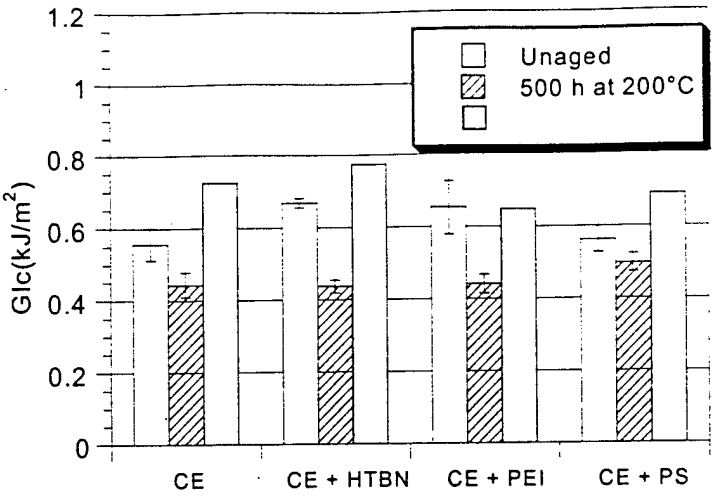

Figure 5 Mode I interlaminar fracture toughness of unaged, thermally aged (in air at 200°C), and conditioned (in water at 95°C) cyanate ester composite materials.

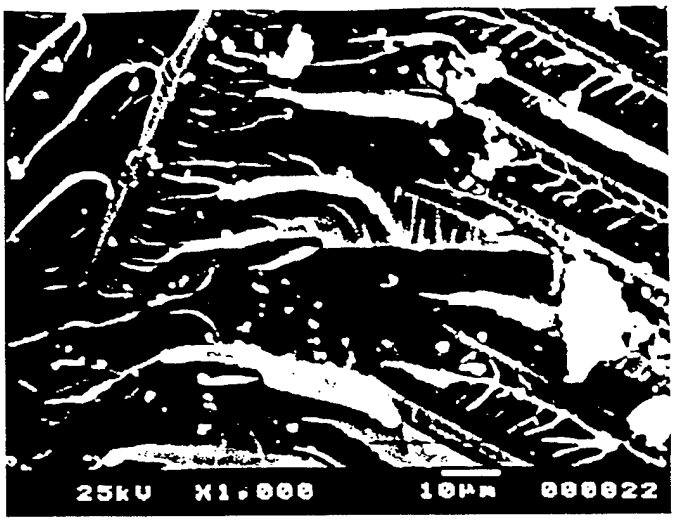

Figure 6 Brittle failure of cyanate ester matrix during mode I interlaminar fracture testing (material: CE + 10 wt% HTBN aged in air at 200°C for 500 hours, by SEM).

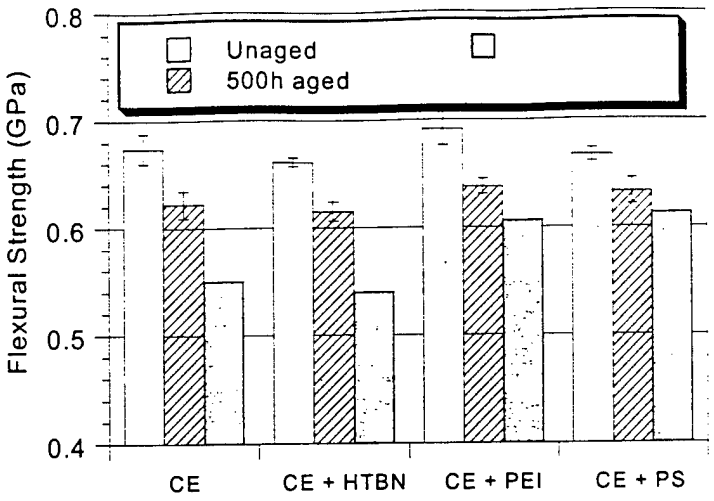

Figure 7 Flexural strength of unaged and aged cyanate ester composite materials (CE) containing different modifiers (aging at 200°C in air, by ASTM D790).

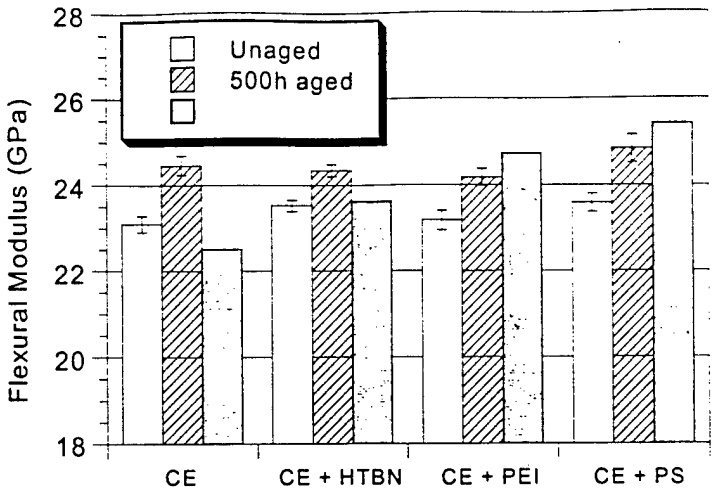

Figure 8 Flexural moduli of unaged and aged cyanate ester composite materials (CE) containing different modifiers (aging at 200°C in air, by ASTM D790).

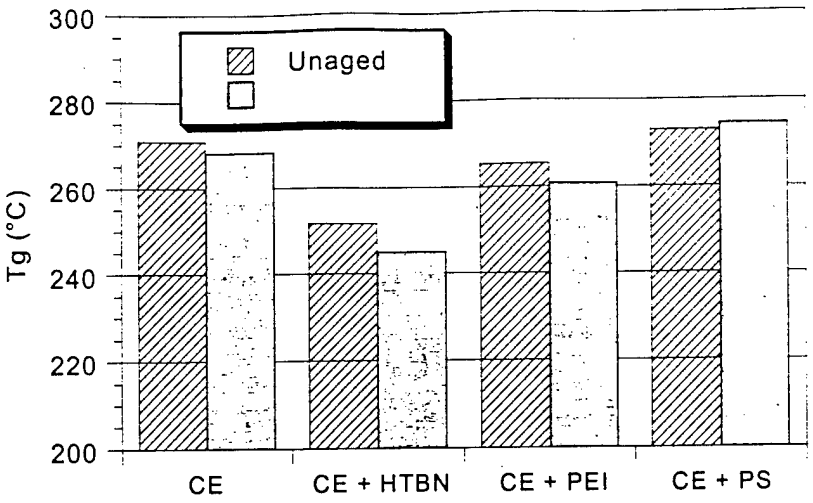

Figure 9 Glass transition temperatures (T_g) of unaged and aged cyanate ester composite materials (CE) containing different modifiers (aging at 200°C in air, by E'' using DMA).

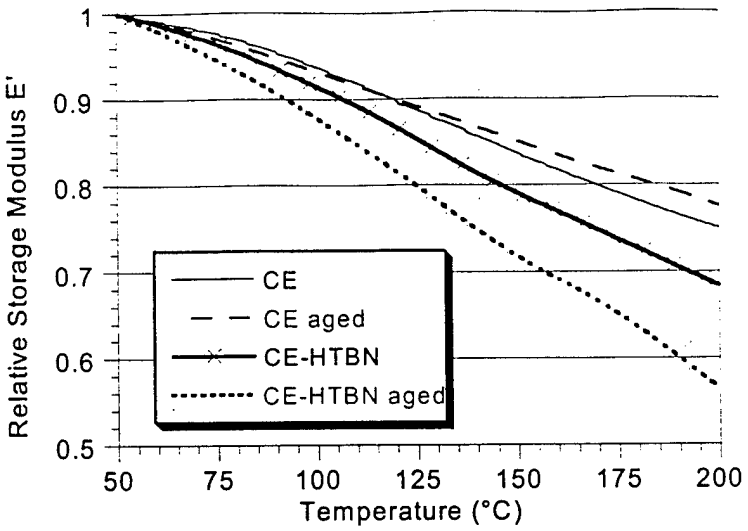

Figure 10 Relative storage moduli (E') of unaged and aged base cyanate ester (CE) and HTBN modified cyanate ester material (aging for 500 hours in air at 200°C, by DMA).

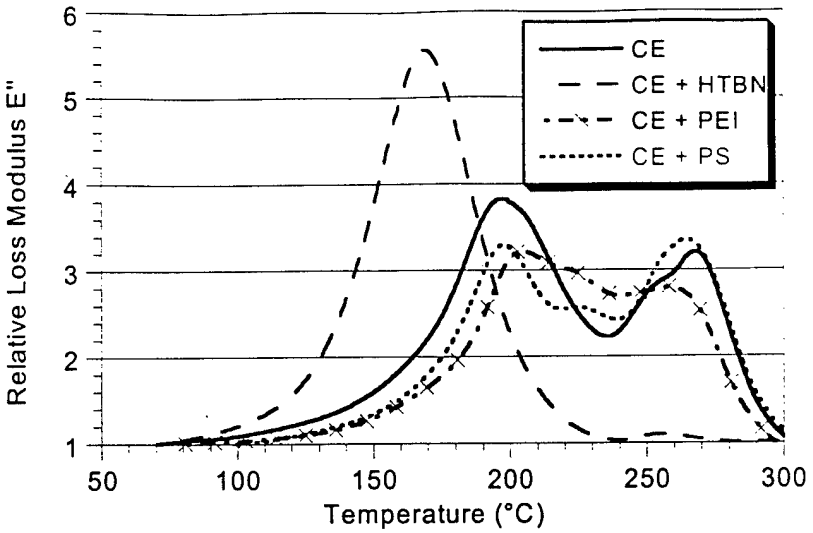

Figure 11 Relative loss moduli (E'') of cyanate ester composite materials (CE) containing different modifiers after 1200 hours aging in air at 200°C (by DMA). All materials exhibit two loss peaks after aging experiments: one close to the peak of unaged material and a second one between 70°C and 100°C below this initial value

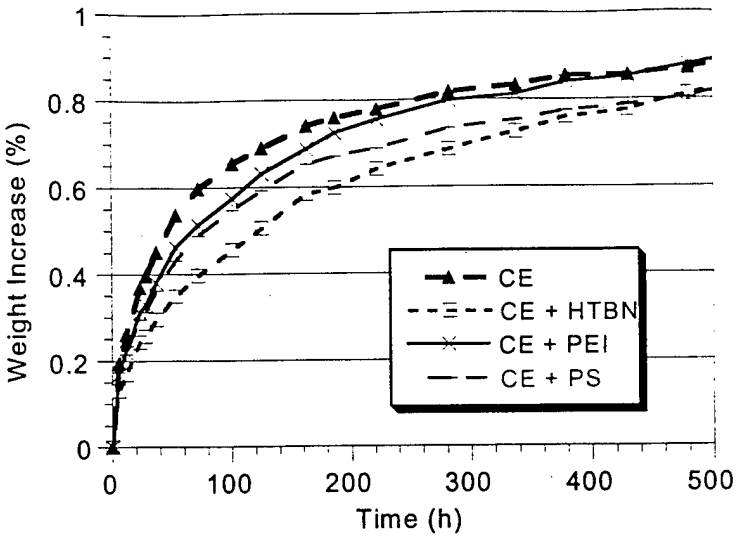

Figure 12 Weight increase due to water absorption of cyanate ester composite materials (CE) containing different modifiers (immersion in 95°C water).

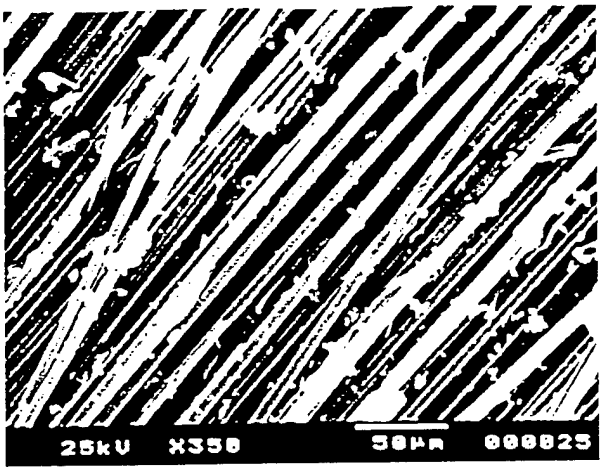

Figure 13 Mode I fracture surface showing large areas of delaminated fibers. Lack of matrix residuals on fiber surfaces indicates poor interfacial adhesion (material: HTBN modified CE, by SEM).

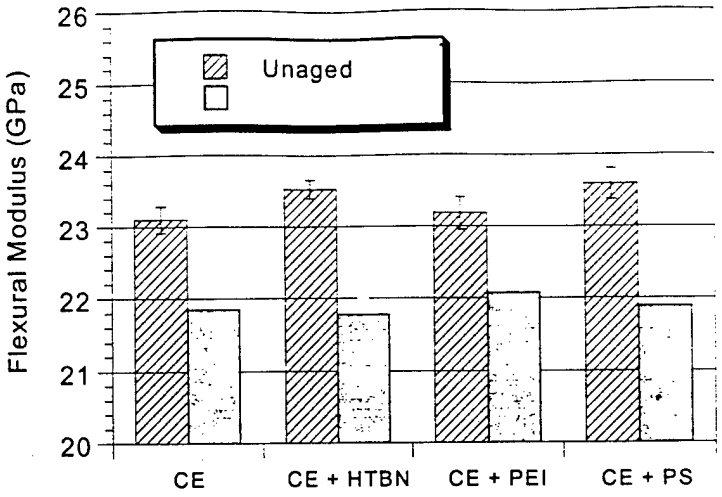

Figure 14 Flexural moduli of unaged and water conditioned cyanate ester materials containing different modifiers (immersion in 95°C water for 500 hours, by ASTM D 790).

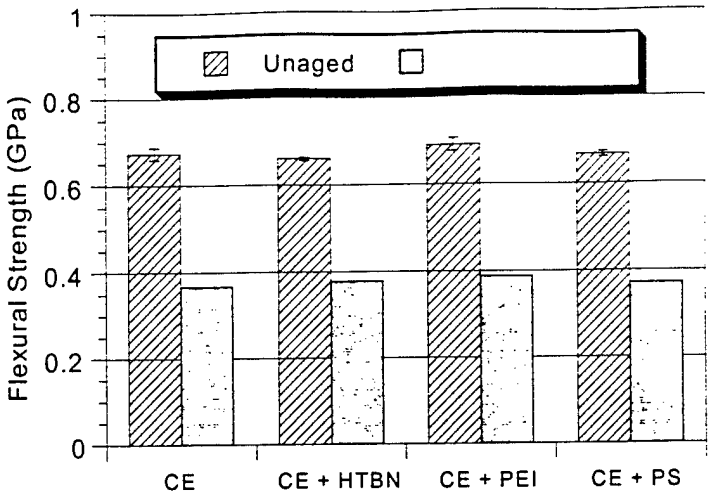

Figure 15 Flexural strength of unaged and water conditioned cyanate ester materials containing different modifiers (immersion in 95°C water for 500 hours, by ASTM D 790).

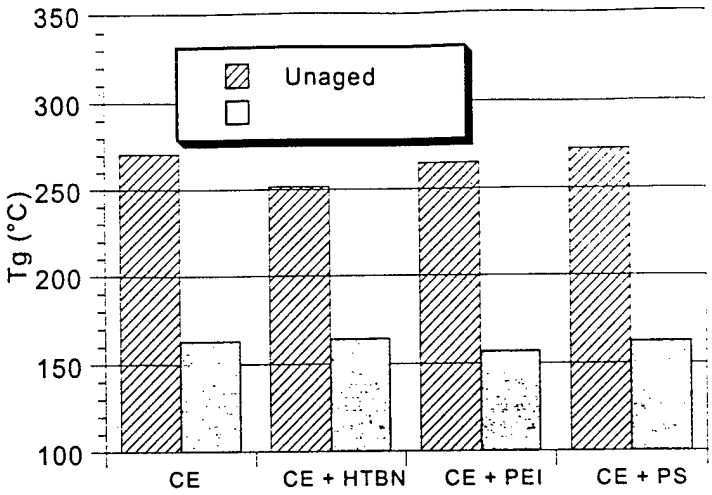

Figure 16 Glass transition temperatures (T_g) of unaged and water conditioned cyanate ester materials containing different modifiers (immersion in 95°C water for 500 hours, by E'' using DMA).

DEVELOPMENT OF THE TRANSIENT SIMULATED LAMINATE (TSL) METHODOLOGY FOR MOISTURE INGRESSION STUDIES USING UNSYMMETRIC LAMINATES

This section presents a non-destructive method to examine a carbon fiber/epoxy composite under hygrothermal conditions. By applying the transient simulated laminate (TSL) technique, a methodology was developed to evaluate the effects of water ingression on the laminates based on the changes in curvatures of laminates. The absorption-desorption-resorption cycle of laminates was evaluated *in situ* by measuring both moisture content and curvatures of unsymmetric laminates $[0_2/90_2]_T$. Curvatures of laminates decreased as more water diffused into the laminate. During hygrothermal cycling, the curvature of a laminate was affected by absorption and desorption temperatures. This study demonstrated that curvature measurements in addition to moisture measurements could be effective tools for relating physical state changes to hygrothermal cycling history in composite laminates.

INTRODUCTION

High-performance fiber reinforced composites have been used in the aerospace industry for many decades. In recent years, they are increasingly being used in the sporting goods and transportation industries. Despite the extensive usage of composite materials in our daily lives, there is a lack of understanding of how environmental exposure, especially humidity and heat cycling, affect long-term properties. It is known that the mechanical and physical properties of polymeric composites change noticeably when plasticization is induced by moisture [1]. The effects are especially detrimental when moisture exposure is combined with high temperature exposure. Irreversible phenomenon, such as microcracking, degradation, and chain scission, are likely to occur in the material.

Accordingly, the study of water diffusion in epoxy materials is important in determining the long-term durability of the material. Many researchers have studied water diffusion in polymeric materials by exposing the material in a controlled moist environment - either in water vapor or liquid water [2-4]. In most of the literature, the

weight change of the material is recorded in a quantitative way to investigate the moisture absorption. The coefficient of water diffusion is then calculated from this information, and the diffusion kinetics are determined. Dynamic mechanical analysis is commonly used to relate moisture solubility and the material properties [5, 6]. The drawback of these studies on water ingression in polymeric materials is the absence of a long-term *in-situ* monitoring method to evaluate changes in the material properties as a function of time or moisture concentration.

It is desirable to develop a non-destructive technique for *in-situ* monitoring of composite specimens subjected to long-term exposure. For example, a non-destructive technique can be effective to compare the hygrothermal effect on a composite material with and without a protective paint coating. In previous work, the process simulated laminate (PSL) technique was developed to investigate the internal residual stresses in the through-thickness direction, that were induced during curing process in the laminate [7]. A PSL consists of a thick laminate (i.e., 40 plies) having separation films placed between certain layers (i.e., every 4 plies) in the laminate. These separation films would enable the division of the laminate after processing. By measuring the curvature of each layer in the laminate after processing, a distribution profile of the internal stresses in the through-the-thickness direction of the laminate can be determined from the curvature calculation. The PSL technique could possibly be modified to relate moisture concentration to material properties.

Difficulties arise when the PSL technique was applied directly for moisture studies. Specifically, the water ingression path would be blocked and disrupted from the separation films. Therefore, a transient simulated laminate (TSL) technique was developed for the water ingression study, which would use similar measurements as the PSL technique. The TSL technique utilizes no separation films and only a thin unsymmetric laminate, similar to one layer (i.e., one 4-ply layer) of the laminate in the PSL technique.

A lay-up configuration that yields a thin unsymmetric laminate was essential for the TSL technique. With this requirement, a square laminate was selected with a $[0_2/90_2]_T$ configuration. The curvature and the shape of this simple configuration have been studied extensively in the literature [8-12]. Classical lamination theory predicts a

saddle shape for all laminates with $[0_2/90_2]_T$ configuration. However, it has been shown that cylindrical shapes are possible for this configuration as well [8]. Saddle shapes are exhibited for small or thick laminates (large thickness to length or width ratio). For large or thin laminates (small thickness to length or width ratio), cylindrical shapes with the well known "snap-through phenomena" are encountered. For example, one can start with a laminate having the curvature along the x-axis. By applying pressure on the center of the laminate, it can "snap-through", and then a laminate which has the curvature along the y-axis results. Therefore, a large, square, unsymmetric laminate with $[0_2/90_2]_T$ configuration would be an excellent tryout for studying moisture ingression with *in-situ* monitoring capability.

Hyer was the first to attempt to predict both the saddle shape and the cylindrical shape of a thin, square, unsymmetric laminate with $[0_n/90_n]_T$ configuration of various side lengths at room temperature in a dry environment. His method consisted of a Rayleigh-Ritz approach, in which the total potential energy was minimized on the stable shape [11]. However, his method could not accurately predict the actual curvatures, although qualitative predictions could be obtained. This was due to many factors, such as laminate size, laminate thickness, mechanical and physical properties of the laminate, autoclave conditions, tooling materials, lay-up, and cooling conditions, that were ignored in the method development [9, 11]. Improvements on this method to account for some of these factors have followed since then [9, 10].

The purpose of this study was to understand the curvature-moisture relationship with *in-situ* monitoring using the TSL technique and to compare the curvature-moisture relationship to that predicted by the model developed in this study. Any physical and mechanical changes in the laminate properties during cycling were assessed and discussed from the knowledge of the curvature-moisture relationship.

THEORETICAL FORMULATIONS

By taking moisture into consideration, predictions of the shapes of unsymmetric laminates become more difficult by model calculations. Therefore, a model predicting curvatures with adequate approximation would be essential for the initial effort. The

model developed in this study neglected the effects of any mechanical constraints during the autoclave and bagging process and assumed that there were no external forces and moments applied during and after cooling. These assumptions were similar to the ones used by Hyer [11].

It was assumed that cured laminates are flat, stress free, and strain free at a given temperature and under dry conditions. This temperature, called the stress free temperature, was selected to be 30 °C below the curing temperature of the resin in the autoclave process. As the laminate cools from the cure temperature to room temperature, an out-of-plane deflection develops from the differences in the thermal expansion properties of each ply. After the laminate cools to room temperature, the out-of-plane deflection changes as the temperature and moisture content of the laminate change. The change in the out-of-plane deflection, induced by the change in moisture content, is brought about by the differences in the moisture expansion properties of each ply. This occurs in the same way as the differences in the thermal expansion cause out-of plane deflections. Since it was assumed that external forces and momentum do not exist during cooling and water absorption, the total potential energy was the same as the total strain energy in the laminate. The total strain energy W was represented as the volume integral of strain energy density ω as follows [11]:

The total strain energy density ω was calculated as follows:

$$\omega = \frac{1}{2}\{\varepsilon\}^T D\{\varepsilon\} - \{\varepsilon\}^T D\{\alpha\}\Delta T - \{\varepsilon\}^T D\{\beta\}\Delta M \qquad (1)$$

$$W = \int_V \omega \, dV \qquad (2)$$

where $\{\varepsilon\}$ is the total strain vector, D is the stiffness matrix of the material, $\{\alpha\}$ is the coefficient of the thermal expansion vector, $\{\beta\}$ is the coefficient of the moisture expansion vector, ΔT is the difference between the stress free temperature and the service temperature, and ΔM is the moisture difference or the moisture concentration in the laminate. In equation (2), the total strain is a linear combination of elastic, thermal, and moisture induced strains. D, $\{\alpha\}$, and $\{\beta\}$ are assumed constant in the range of temperature and moisture concentration experienced in this study [13].

The weight change, ΔM, due to the moisture ingression in laminate, was defined as follows:

$$\Delta M(\%) = \frac{m - m_0}{m_0} \times 100 \tag{3}$$

where m is a transient weight, and m_0 is the initial weight of a laminate in each sorption step.

In order to formulate the strains in the material, the in-plane and out-of-plane deflections in the mid-plane of a laminate, using global coordinates, were assumed as follows:

$$\begin{aligned} u &= cx - \frac{a^2x^3}{6} - \frac{abxy^2}{4} \\ v &= dy - \frac{b^2y^3}{6} - \frac{abx^2y}{4} \\ w &= \frac{1}{2}\left(ax^2 + by^2\right) \end{aligned} \tag{4}$$

In equations (4), a, b, c, and d are constants to be determined; u, v, and w are deflections of the mid-plane in x, y, and z directions of global coordinates, respectively. Both the saddle shape and the cylindrical shape of an unsymmetric laminate can be predicted from the expressions in equation (4). A saddle shape solution is described when a equals $-b$. When a or b equals zero, a cylindrical shape solution is described. The two solutions, a=0 or b=0, show a "snap-through" phenomenon, which means that one shape could be snapped into another shape. The deflections are assumed as in equation (4) because the in-plane strains are similar to the predictions of classical lamination theory, which are independent of x and y, with no in-plane shearing strain. Using equation (4), the strains in mid-plane are given as follows:

$$\begin{aligned} \varepsilon_x^0 &= \frac{\partial u}{\partial x} + \frac{1}{2}\left(\frac{\partial w}{\partial x}\right)^2 = c - \frac{aby^2}{4} \\ \varepsilon_y^0 &= \frac{\partial v}{\partial y} + \frac{1}{2}\left(\frac{\partial w}{\partial y}\right)^2 = d - \frac{abx^2}{4} \\ \varepsilon_{xy}^0 &= \frac{1}{2}\left(\frac{\partial u}{\partial y} + \frac{\partial v}{\partial x} + \left(\frac{\partial w}{\partial x}\right)\left(\frac{\partial w}{\partial y}\right)\right) = 0 \end{aligned} \tag{5}$$

The strains at any point in the laminates, which are based on von Karaman plate theory, are given as follows [11]:

$$\varepsilon_x = \varepsilon_x^0 - z\frac{\partial^2 w}{\partial x^2} = c - \frac{aby^2}{4} - az$$
$$\varepsilon_y = \varepsilon_y^0 - z\frac{\partial^2 w}{\partial y^2} = d - \frac{abx^2}{4} - bz \qquad (6)$$
$$\varepsilon_{xy} = \varepsilon_{xy}^0 - z\frac{\partial^2 w}{\partial x \partial y} = 0$$

Equation (2) is then expanded and substituted by equation (6) as follows:

$$\omega = \frac{1}{2}\overline{Q}_{11}\varepsilon_x^{\,2} + \overline{Q}_{12}\varepsilon_x\varepsilon_y + \frac{1}{2}\overline{Q}_{22}\varepsilon_y^{\,2}$$
$$-\left(\overline{Q}_{11}\alpha_x + \overline{Q}_{12}\alpha_y\right)\varepsilon_x\Delta T - \left(\overline{Q}_{12}\alpha_x + \overline{Q}_{22}\alpha_y\right)\varepsilon_y\Delta T \qquad (7)$$
$$-\left(\overline{Q}_{11}\beta_x + \overline{Q}_{12}\beta_y\right)\varepsilon_x\Delta M - \left(\overline{Q}_{12}\beta_x + \overline{Q}_{22}\beta_y\right)\varepsilon_y\Delta M$$

In equation (7), $\overline{Q}_{ij}$ is the reduced stiffness, α_x, α_y are the coefficients of thermal expansion in the x-direction and y-direction, and β_x, β_y are the coefficients of moisture expansion in the x-direction and y-direction. For this laminate, it is reasonable to assume α_{xy} and β_{xy} are both zero. According to the Rayleigh-Ritz method, when the first variation of the total strain energy equals zero, the total strain energy becomes minimized and it the gives the upper-estimated solution. The first variation is given as follows:

$$\delta W = \left(\frac{\partial W}{\partial a}\right)\delta a + \left(\frac{\partial W}{\partial b}\right)\delta b + \left(\frac{\partial W}{\partial c}\right)\delta c + \left(\frac{\partial W}{\partial d}\right)\delta d \equiv 0 \qquad (8)$$

which leads to the next four equations, shown in equation (9).

$$\left(\frac{\partial W}{\partial a}\right) = 0,\ \left(\frac{\partial W}{\partial b}\right) = 0,\ \left(\frac{\partial W}{\partial c}\right) = 0,\ \left(\frac{\partial W}{\partial d}\right) = 0 \qquad (9)$$

By solving these four equations, the constants *a*, *b*, *c*, and *d* are determined. The curvatures of a laminate, κ_x, κ_y, and κ_{xy}, are given as follows:

$$\kappa_x = \frac{\partial^2 w}{\partial x^2} = a, \quad \kappa_y = \frac{\partial^2 w}{\partial y^2} = b, \quad \kappa_{xy} = \frac{\partial^2 w}{\partial x \partial y} = 0 \qquad (10)$$

EXPERIMENTAL

Material

A commercial grade carbon fiber/epoxy unidirectional prepreg (Cytec-Fiberite HYE970/T300) was used for the hygrothermal studies. Resin content was measured by the solvent extraction method and experimentally determined to be 37 %. Laminates were made using the recommended cure cycle, which included a curing temperature of 177 °C for two hours and a pressure of 552 kPa (80 psi). The properties of this laminate are listed as follows:

E_L = 124 GPa ;E_T = 8.6 GPa ;ν_{LT} = 0.28 ;G_{LT} = 6.0 GPa.

The model computations also require values of physical properties (α_L, α_T, β_L, and β_T) of the laminate. These values were evaluated experimentally and described below.

Water Diffusion Experiment

Moisture sorption studies were performed with non-symmetric laminates $[0_2/90_2]_T$ approximately 15 x 15 x 0.08 cm in size. A total of nine laminates were used in this study. Prior to experiment, the four edges of the laminate were polished to give straight lines with right angles and smooth surfaces. The surfaces were then cleaned with methanol. Samples were dried at 40 °C in an oven with desiccant for three days to obtain an initial reference of moisture condition. Samples were subsequently immersed in liquid water held at a constant temperature. All sorption experiments were conducted in de-ionized water. Three temperatures were used: 28, 50, and 80 °C. When pseudo-equilibrium was reached, samples were taken out of the water baths and placed in constant temperature ovens with desiccant for the desorption step. Three temperatures, room temperature, 50 °C, and 80 °C, were used in the desorption step. Desorption at room temperature was accomplished by placing the samples in a desiccator. The room temperature was approximately 22 °C. When the mass of the sample approached a constant value, samples were put back into water baths again for resorption at three

temperatures, 28, 50, and 80 °C. Therefore, all samples went through the "abs-des-res" (absorption-desorption-resorption) segments in the sorption study.

Sample weights and curvatures were recorded periodically at room temperature throughout the experiments by removing the samples from the water baths, and then blotting them dry, or by removing samples from ovens and cooling them to ambient temperature. It was essential to perform all measurements at the same temperature (ambient temperature in this case) so that model calculations could be simplified and the data compared. Sample weight was measured on an analytical balance accurate to 0.0001 g. The displacements of the principal curvature were measured from the height and the base of the arc using a measuring device accurate to 0.5 mm. The cylindrical curvature is then calculated as follows:

$$\kappa = \frac{8h}{l^2 + 4h^2} \tag{11}$$

where κ is the curvature (or the inverse of the radius) of the sample, h is the arc height, and l is the base length as shown in Figure 1.

Physical Properties Measurement

Although the system used is a commercial grade, some parameters are not available in the literature. These parameters were evaluated in our laboratory for the model prediction calculations. The coefficient of thermal expansion (α) and the coefficient of moisture expansion (β) of the material in both the longitudinal and transverse directions were determined experimentally. α was determined by measuring the dimensional changes of a 26-ply, unidirectional laminate using a thermomechanical analyzer (TA Instrument TMA 2940) with a macro-expansion probe. A static force of 0.1 N and various heating rates ranging from 1 to 5 °C/min were used to extrapolate α at zero heating rate. β was calculated by measuring the dimensional changes and the weight gain of submerged 14 x 14 cm, four-ply, unidirectional laminates in water baths at 28, 50, and 80 °C. Before placement in the water bath, each laminate was prepared the same way the sorption laminates were, as described previously. During measurements, samples were taken out of the water bath and blotted dry. The dimensions of samples

were measured at room temperature to within 0.01 mm accuracy and the sample weights were obtained from an analytical balance accurate to 0.0001 g.

RESULTS AND DISCUSSIONS

Physical Property Evaluation

The coefficients of thermal expansion for this material were found to be 3.57 x 10^{-6} $°C^{-1}$ in the longitudinal direction (α_L) and 4.96 x 10^{-5} $°C^{-1}$ in the transverse direction (α_T) extrapolated at zero heating rate, over a temperature range of 25 to 100 °C. The coefficients of moisture expansion were determined from the slope of the dimension change as a function of moisture content. It was assumed that dimensional changes in the sample thickness direction were negligible. β_L was found to be zero at all moisture contents. In the transverse direction, β_T was found to be 0.34 cm/cm-moisture, independent of the water bath temperature. The calculated β_T was valid up to a 1.6 % moisture content. At a moisture content higher than 1.6%, β_T was approximately zero.

Data Trends

An example of the experimental data is shown in Figure 2. This figure shows the dependence of moisture and curvature on time during data collection when the laminate underwent the "abs-des-res" steps. The laminate experienced weight gain in the absorption and resorption steps as more water molecules diffused into the laminate structure. Consequently, the structure became more relaxed and resulted in a decrease in the curvature value. In the desorption step, the laminate showed opposite behavior, i.e. it lost weight, and showed an increase in the curvature value. The weight loss in the desorption step usually exceeded the weight gain in the absorption step. Water diffusion in the laminates was faster in the resorption step than in the absorption step. In addition, note that in Figure 2 the laminate reached its ultimate curvature value more quickly than the moisture. This was especially apparent in the absorption step. The observations of higher a value of M_∞ at a higher absorption temperature, and a larger amount of weight loss in the desorption than weight gain in the absorption, were also noted in the literature[1, 5]. Seferis et al and Nicolais et al attributed these observations to the removal

of unattached, low molecular-weight molecules from the matrix during the absorption process.

During the experiments, it was noticed that as more water diffused into the laminate, the actual shape of the laminate became more difficult to determine. This was because the laminate became almost flat at the highest moisture content. It was then difficult to distinguish between flat, slightly cylindrical, and slightly saddle shape. A high percentage of error could have occurred during the measurement as well since the arc length of the laminate was small and close to the sensitivity level of the measuring device.

Moisture-Time Relationship

The moisture-time relationship was used to determine the sorption kinetics via the Fickian diffusion model. Figure 3 shows the water ingression behavior in the absorption step by measuring the weight change as time increases. Non-Fickian diffusion was not observed in this study, although many references sited such observation with particular resin systems or at higher moisture ranges[3, 5, 14, 15]. It is shown clearly in Figure 3 that water diffused into the laminate and reached equilibrium faster at higher absorption temperatures. The parameters of absorption kinetics, equilibrium water content (M_∞), and diffusivity were determined from the best fit to the absorption curve with constraints from the initial slopes of the absorption data. The best fits, shown in Figure 3 as the solid lines, described the data adequately over most of the range. Table 1 shows the absorption parameters calculated in this study. In Table 1, the M_∞ and diffusivity are larger at a higher absorption temperature, corresponding to what was observed in Figure 3.

In addition, the resorption parameters were calculated using the same method, as shown in Table 2. Notice that at each resorption temperature, the values of M_∞ and diffusivity in the resorption step are the same as or greater than the values of the same temperature in the absorption step (Table 1). It is clear from Table 2 that the kinetic parameters for resorption were dependent on the hygrothermal history. Variations of "abs-des" combinations affected the water sorption kinetics parameters in the resorption step. For example, in the 80 °C resorption case, the sample that experienced low "abs-des" temperature (such as 28-22) resulted in a lower M_∞ than the sample that experienced

high "abs-des" temperatures (such as 80-80). The high absorption temperature seemed to be a significant factor in the sorption study, however, desorption temperature also was important.

Three sets of resorption data in which samples were equilibrated at 50 °C before drying at 80 °C (50-80-res) are plotted in Figure 3-4. The calculated values of M_∞ and diffusivity are listed in Table 2 as samples 50-80-28, 50-80-50, and 50-80-80. In Figure 4, it is seen that as the resorption temperature increased, the diffusivity increased, but the equilibrium water content did not change. Comparing Figures 3 and 4 shows that the diffusion rate for each sorption temperature in the resorption step increased significantly than the absorption step. Consequently, M_∞ for each sorption temperature in the resorption step reached approximately the same value which exceeded the values in the absorption step. In addition, the Fickian diffusion assumption appears to be more representative than in the absorption case (Figure 3).

Curvature Behaviors

Using the TSL technique, the model developed in this study calculated the curvatures of the laminate under dry conditions as shown in Figure 5. The predictions at $\Delta M = 0$ correspond to the ones predicted by Hyer [11]. Figure 5 shows that the critical length is 42 mm. A sample size less than this critical length would exhibit a saddle shape following the curvature values from point A to point B in Figure 5. A sample size larger than this critical length would show a cylindrical shape following the curvature values (in x direction) from point B to C in Figure 5. Note that for a sample size greater than the critical length, two other solutions are also shown in Figure 5 in addition to curve BC. Curve BD is the theoretical saddle shape of the laminate, however, this solution is not stable and does not show in experimental observations. Curve BE is the curvature in y direction (~ 0) of the laminate when the laminate has a cylindrical shape in the x direction (curve BC). The curvature for the "snap-through" phenomenon in the other direction is symmetrical to Figure 5 and is not shown here. Figure 6 is the model prediction for the laminate at $\Delta M = 1.0$ %. At $\Delta M = 1.0$ %, the critical length increases to 60 mm. Curves AB, BC, BD, and BE in Figure 6 represent similar behaviors as in Figure 5. For this study, a sample size of 15 cm (150 mm) is always greater than the critical length

according to the model prediction. Taking the curvature value at each ΔM point, a curvature-moisture relationship can be determined for a laminate of the same size. This relationship is shown as the solid line in Figure 7. In this numerical simulation, the hygrothermal cycling effects are not considered; therefore, only one curvature-moisture relationship is predicted.

The experimental values of initial curvature for laminates at zero time in the absorption step were calculated to be 4.5 ± 0.4 m^{-1}. The deviations may be caused from slight variations in sample sizes and autoclave conditions from batch to batch. One batch of autoclaved samples showed consistently lower initial radii of curvature than other batches. A predicted curvature value using the method developed, however, is 6.2 m^{-1} for a sample size of 150 mm square with zero moisture, as shown in Figure 5. The predicted curvature is almost 40% higher than the actual values. Differences in the absolute values were expected since many factors were not accounted for in the model. For better comparisons between laminates and model prediction, the relative curvature change ($\Delta\kappa$) is reported instead of the absolute curvature values:

$$\Delta\kappa(\%) = \frac{\kappa - \kappa_0}{\kappa_0} \times 100 \qquad (12)$$

where κ is the curvature of the laminate at a given moisture concentration and κ_0 is the initial curvature of a laminate in each sorption step.

As the laminate became plasticized during water absorption the laminate relaxed and curvature decreased. This correlation for the absorption step is shown in Figure 7. From a weight change of 0 to 1%, the curvature-moisture relationship followed a straight line with the slopes changing with absorption temperatures. Samples subjected to higher absorption temperatures were curved more than the samples in the lower absorption temperature at the same moisture concentration ΔM. This trend resulted in a lower value of slope for a high sorption temperature, as shown in Figure 7. The linear trend changed at high moisture content, especially for samples exposed to the high absorption temperatures. In the high moisture content region, the test specimens reached a steady curvature as more water was absorbed. For example, in the 80 °C absorption, the slope of the curve started to decrease at moisture content of 1%. The curvature values became

constant after a moisture content of 1.5% was reached. In the 50 °C absorption, the slope of the curve was constant until a moisture content of 1.3% was reached. In the 28 °C absorption, the curvature-moisture relationship was linear in all the moisture data range.

The curvature-moisture correlation for the resorption step in which samples underwent an absorption temperature of 50 °C and a desorption temperature of 80 °C (50-80-res) is plotted in Figure 8. Figure 8 shows the same general trends for the resorption step as in Figure 7 for the absorption step but with fewer differences in the slope deviations. Another interesting note when comparing these two figures is that similar curvature values were observed at the high moisture content regions for the samples in the 80 °C and in the 50 °C absorption and resorption cases. The calculated slopes of each curvature-moisture relationship are also shown in Table 3. In Table 3, the values shown are the absolute values of the slopes of the curves in Figures 7 and 8 from 0 to 1 % moisture, using a least-square fit. The absolute value of the slope decreased as the sorption temperature decreased. This was especially apparent in the absorption step. In addition, the absolute value of the slope in the resorption step was lower than the model prediction and lower than the absorption steps for the three sorption temperatures tested.

Water Influences on Structure Changes

The discrepancies seen in Figures 3 and 4, and Figures 7 and 8 suggest that sorption temperature may affect the water-composite interaction in the laminate significantly. Water diffusing through the laminate would experience various regions such as matrix areas with higher and lower crosslink density regions and through fiber beds or in the matrix-interface region. Cycling and sorption temperature is suspected to cause structural changes and molecular rearrangements in neat resins [1, 4, 5]. It is possible that structural changes and molecular rearrangement could also occur in a composite material. The matrix may become more highly crosslinked as it is plasticized during water absorption. Higher crosslink density in the matrix areas would reduce the diffusion rate of water absorption. In addition, diffusion paths along the fibers would be different than the paths in the matrix area. Drying the laminate in the desorption process at different temperatures would cause water desorped through a laminate in various paths

due to the variations in the internal structures of the material. Paths established by desorption became accessible for resorption which resulted in faster diffusion rate and higher equilibrium concentration.

Furthermore, the diffused water may act on the laminate differently to cause the variations observed in the curvature-moisture data. Several authors discussed the two ways that water may be associated with the molecular networks of the matrix[1, 5, 16]. For example, water may diffuse into a laminate without changing the microscopic network of the matrix (i.e., reversible). Or, water may diffuse into a laminate and result in irreversible changes in the matrix. Adamson describes these two types of water influences as "bound" and "unbound" water[16]. Water could "bind" to the composite materials ("bound water) which could affect the physical state of the material. Or water may accumulate within the free volume voids and along the established paths as "unbound" water which could not affect the physical state of the material. The variations shown in Table 2 could result from the amount of "bound" and "unbound" water in the test specimens. The amount of "bound" and "unbound" water was not the same in each sample that experienced a different hygrothermal history. It was suspected that samples that experienced a high temperature absorption and/or desorption were able to hold more water in both the "bound" or "unbound" state and therefore the M_∞ are higher than other samples in the resorption step.

Issues of micro cracks caused by water ingression were explored. However, microscopic analysis on sample surfaces and cross sections detected no visible cracks.

CONCLUSIONS

Environmental exposure of composite materials has been known to degrade and deteriorate their structure. The transient simulated laminate (TSL) technique developed in this study, incorporated a thin unsymmetric laminate as the test object to achieve non-destructive monitoring. The model developed for the TSL technique predicted the curvature-moisture relationship using the Rayleigh-Ritz method.

It was found that curvature measurements provided additional information on the insight of material behavior besides the moisture measurements. During absorption, the diffusivity and equilibrium water content increased with increasing absorption

temperature. Curvature values decreased as more water diffused into the laminate until a constant value was reached. Samples curved more in the high absorption temperature region than in the low absorption temperature region at the same moisture content.

In resorption, water diffusion and curvature behaviors varied depending on the hygrothermal history. The hygrothermal cycling – both absorption and desorption – affected the physical state of a laminate, as determined by moisture and curvature measurements. However, unlike absorption, samples showed approximately the same curvature at all three resorption temperatures at the same moisture content when samples were subjected to the same absorption-desorption path. Water-induced changes in the physical state of the laminate, such as the crosslink density and the presence of diffusion paths, may result in the variations seen from the diffusion and curvature data in this study. This work establishes the initial framework required to provide a non-destructive monitoring technique.

REFERENCES

1. Apicella, A., L. Nicolais, G. Astarita, and E. Drioli, Polymer, **20** 1143 (1979).
2. Sullivan, J.L., Composites Science and Technology, **39** 207 (1990).
3. Foch, B.J. and H.L., McManus. Proceedings of ICCM-11, Gold Coast, Australia, 432 (1997).
4. Wong, T.C. and L.J. Broutman, Polymer Engineering and Science, **25** (9) 521 (1985).
5. Mikols, W.J., J.C. Seferis, A. Apicella, and L. Nicolais, Polymer Composites, **3** (3) 118 (1982).
6. Hiroshi Fujita and A. Kishimoto, Journal of Polymeric Science, **28** 547 (1958).
7. Manson, J.E. and J.C. Seferis, Journal of Composite Materials, **26** (3) 405.
8. Mallick, P.K., Example 3.14, Fiber-reinforced composites: materials, manufacturing, and design, New York: Marcel Dekker, Inc., 178 (1993).
9. Cho, M., *et al.,* Journal of Composite Materials, **32** (5) 460 (1998).
10. Dano, M.-L. and M.W. Hyer, International Journal of Solids Structures, **35** (17) 2101 (1998).
11. Hyer, M.W., Journal of Composite Materials, 15(July) 296 (1981).
12. Hyer, M.W., Journal of Composite Materials, 15(March) 175 (1981).
13. Takatoya, T., K. Chung, Y.-J. Wu, and J.C. Seferis, Proceedings of ICCM-12, Paris, under Durability and Aging (1999).
14. Chateauminois, A., B. Chabert, J.P. Soulier, and L. Vincent, Composites, **24** (7) 547 (1993).
15. Cai, L.-W. and Y. Weitsman, Journal of Composite Materials, **28** (2) 130 (1994).
16. Adamson, M.J, Journal of Materials Science, **15** 1736 (1980).

Table 1 Percentage moisture uptake and diffusion coefficient as evaluated from the absorption study.

Absorption temperature (°C)	M_∞ (%)	DIFFUSIVITY (cm^2/min)
28	1.43 ± 0.01	$(2.92 \pm 0.24)x10^{-8}$
50	1.62 ± 0.06	$(1.04 \pm 0.17)x10^{-7}$
80	1.84 ± 0.03	$(4.76 \pm 0.23)x10^{-7}$

Table 2 Percentage moisture uptake (M_∞) and diffusion coefficient as evaluated in resorption step based on hygrothermal history dependence.

Abs-des-res (°C)	M_∞ (%)	Diffusivity (cm^2/min)
28 °C resorption		
28-50-28	1.74	2.99×10^{-8}
50-80-28	2.10	3.59×10^{-8}
80-50-28	2.15	7.57×10^{-8}
50 °C resorption		
50-50-50	1.68	1.54×10^{-7}
50-80-50	2.08	9.90×10^{-8}
80 °C resorption		
28-22-80	1.98	4.30×10^{-7}
28-50-80	1.95	4.55×10^{-7}
50-80-80	2.14	5.66×10^{-7}
80-80-80	2.22	10.6×10^{-7}

Table 3 Slope of the curvature - moisture line (% $\Delta\kappa$ / % ΔM). Values presented are the absolute values of the actual slope.

	Absorption	Resorption (50-80-res)
Model Prediction	56	56
28 °C	88	49
50 °C	67	45
80 °C	51	42

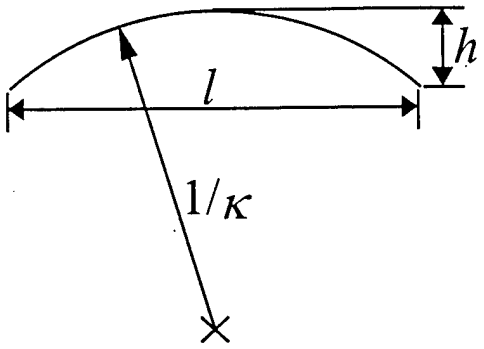

Figure 1 Schematic diagram of cylindrical shaped curvature.

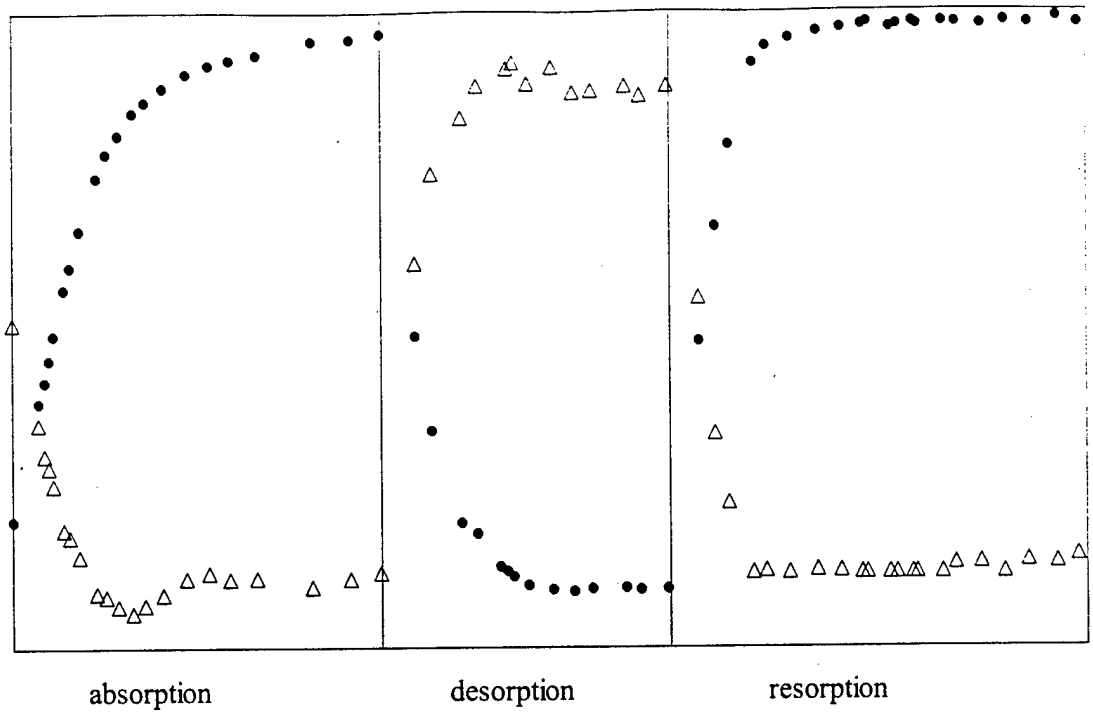

Figure 2 A typical absorption-desorption-resorption curve of the experiment. The x-axis has the unit of (time$^{0.5}$ / laminate thickness) and the data (•) is weight change (%) and the data (Δ) is curvature (length^{-1}).

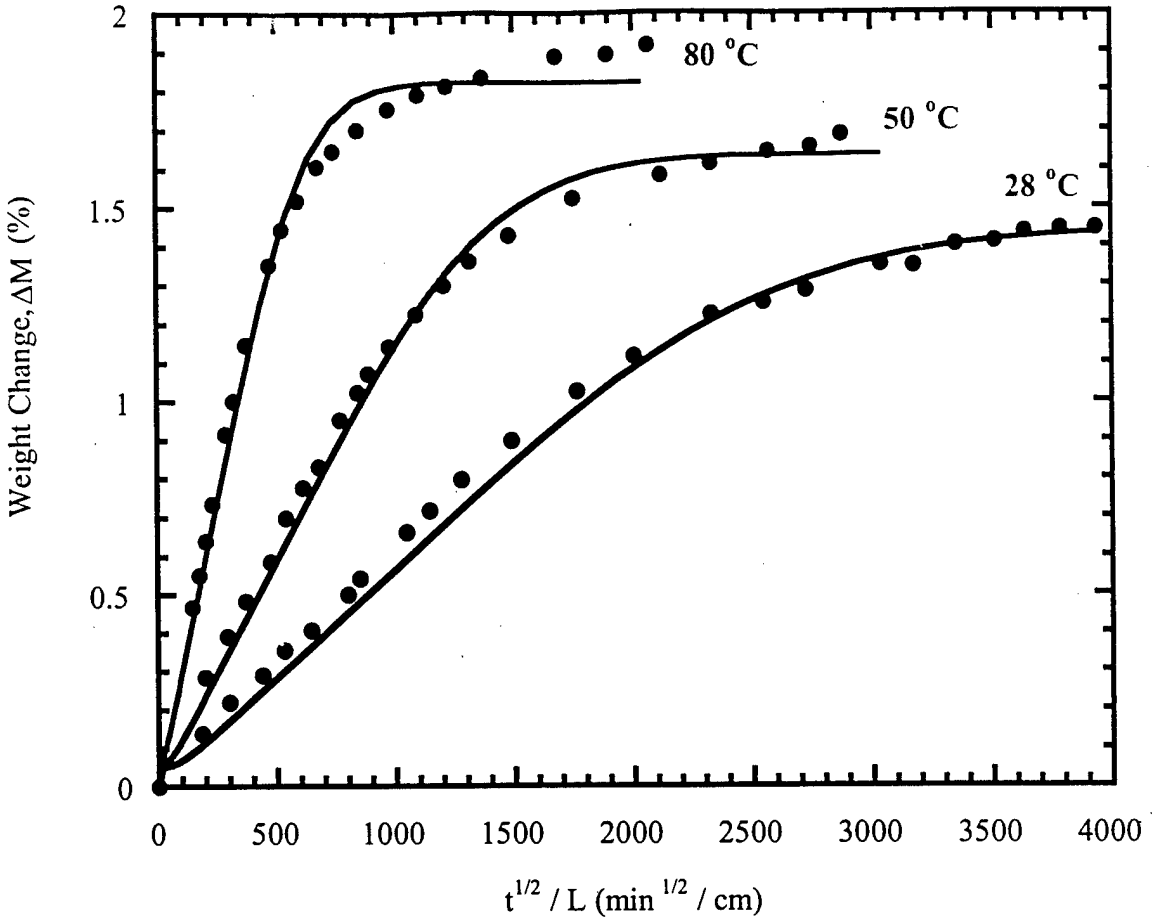

Figure 3 Relationship of moisture content with respect to time of laminates in the absorption step.

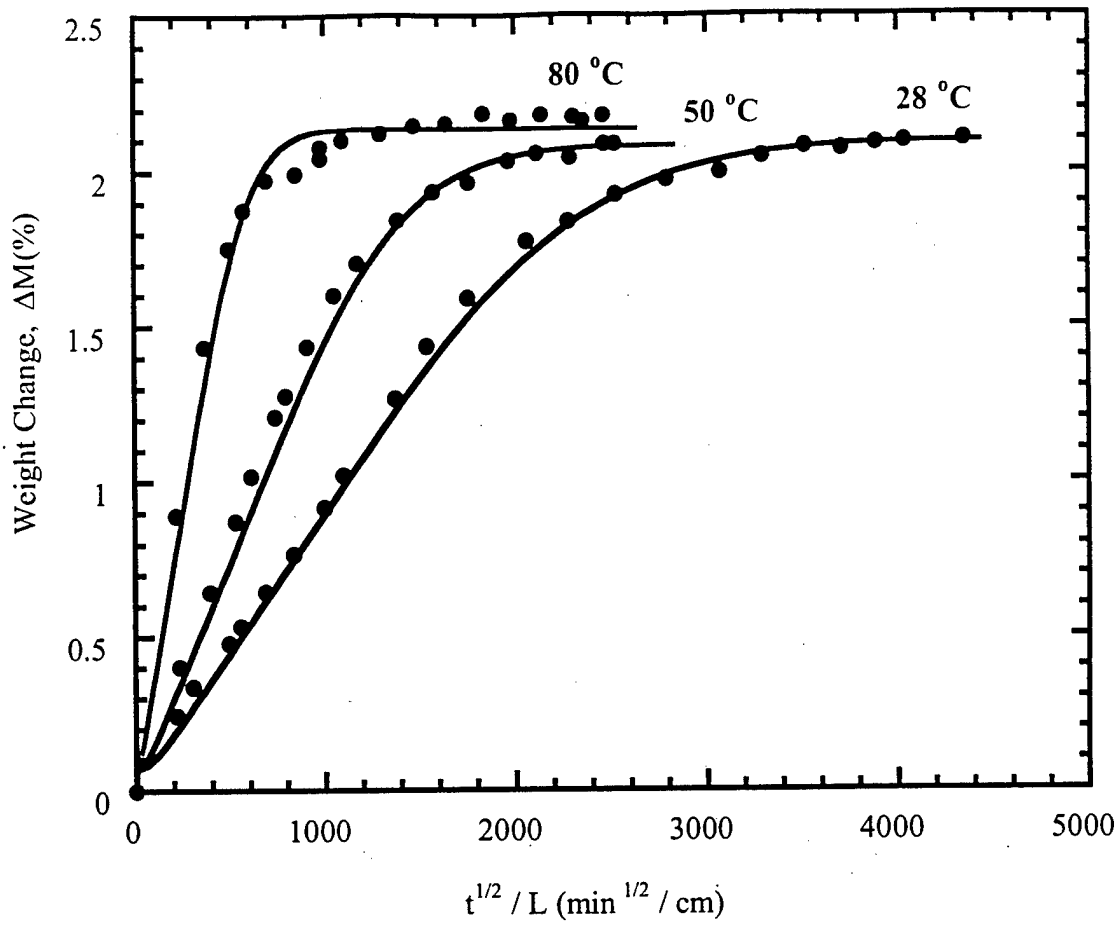

Figure 4 Relationship of moisture content with respect to time of laminates in the resorption step where samples were conditioned through a 50 °C absorption and a 80 °C desorption before the resorption step (50-80-res).

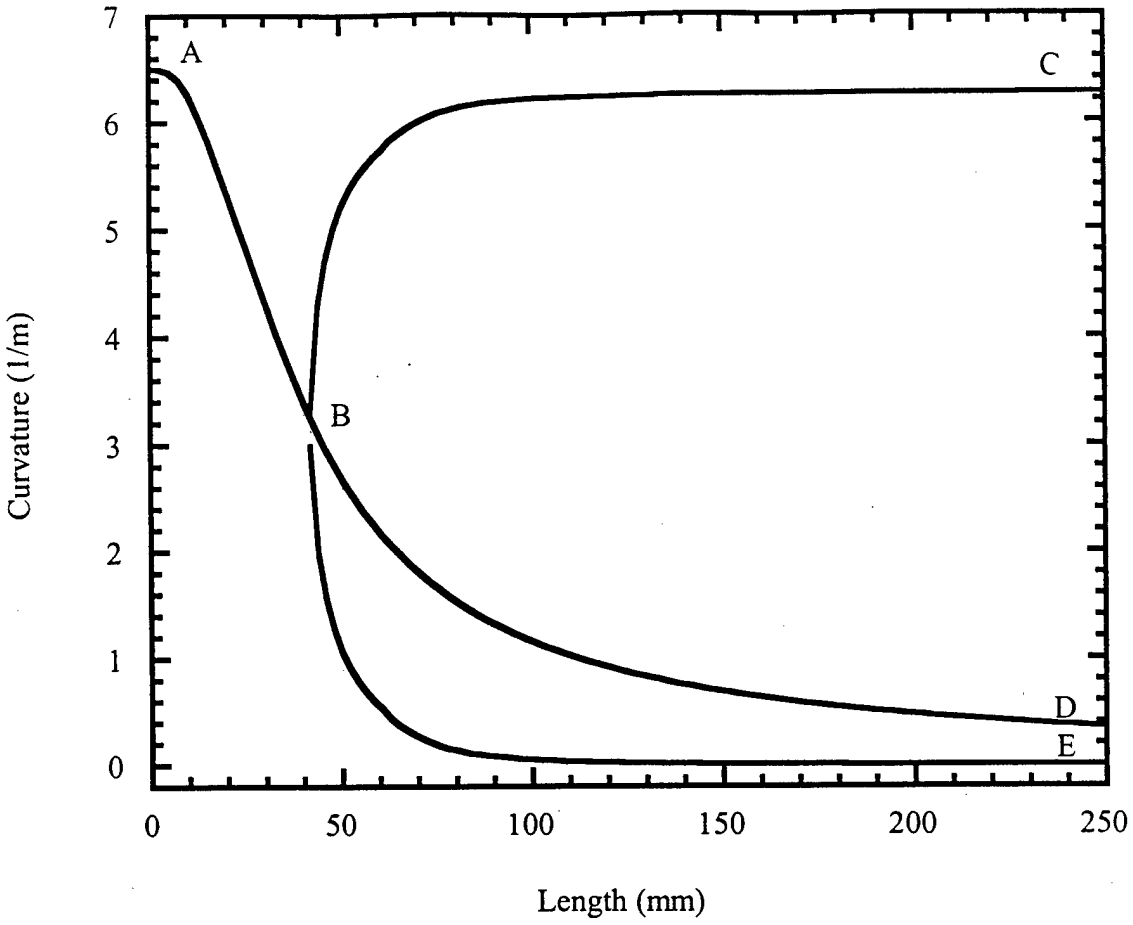

Figure 5 Model prediction of curvature values for various sample size under dry condition ($\Delta M = 0\%$).

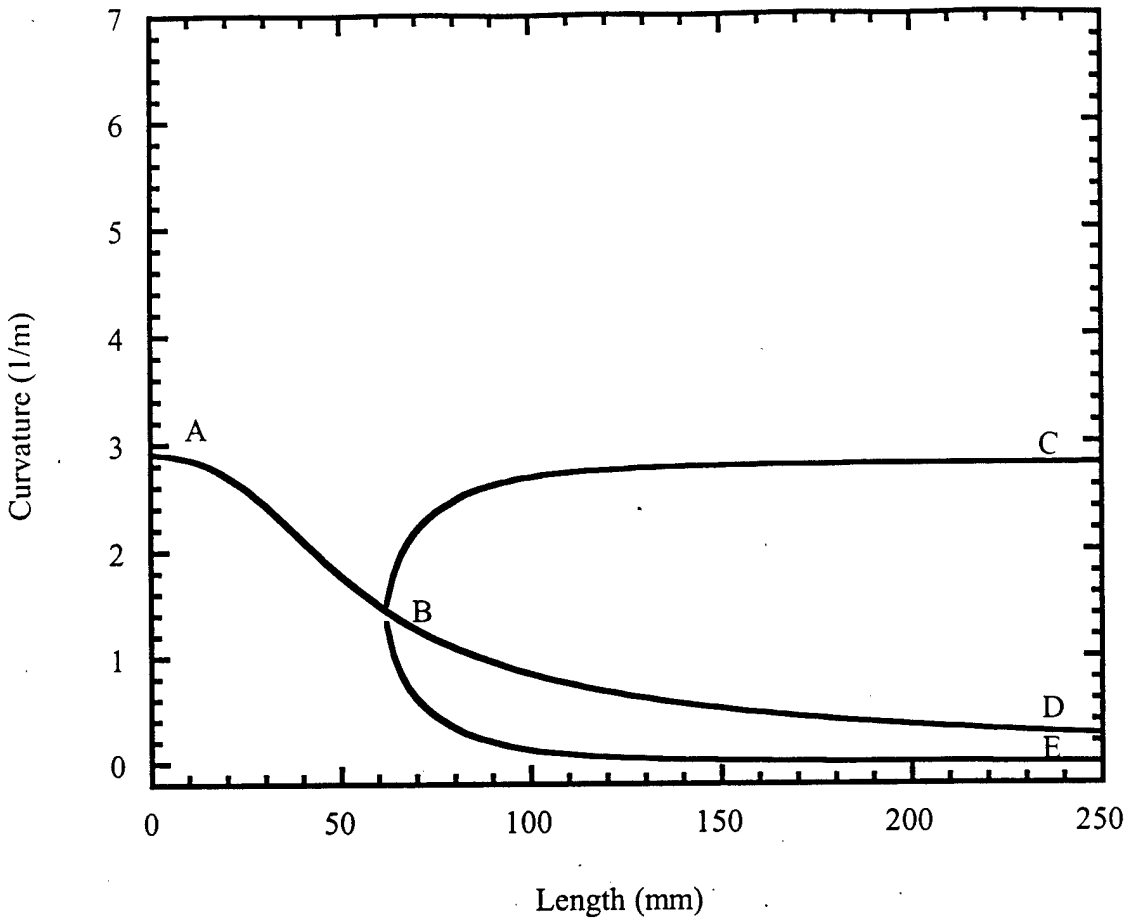

Figure 6 Model prediction of curvature values for various sample size at $\Delta M = 1\%$.

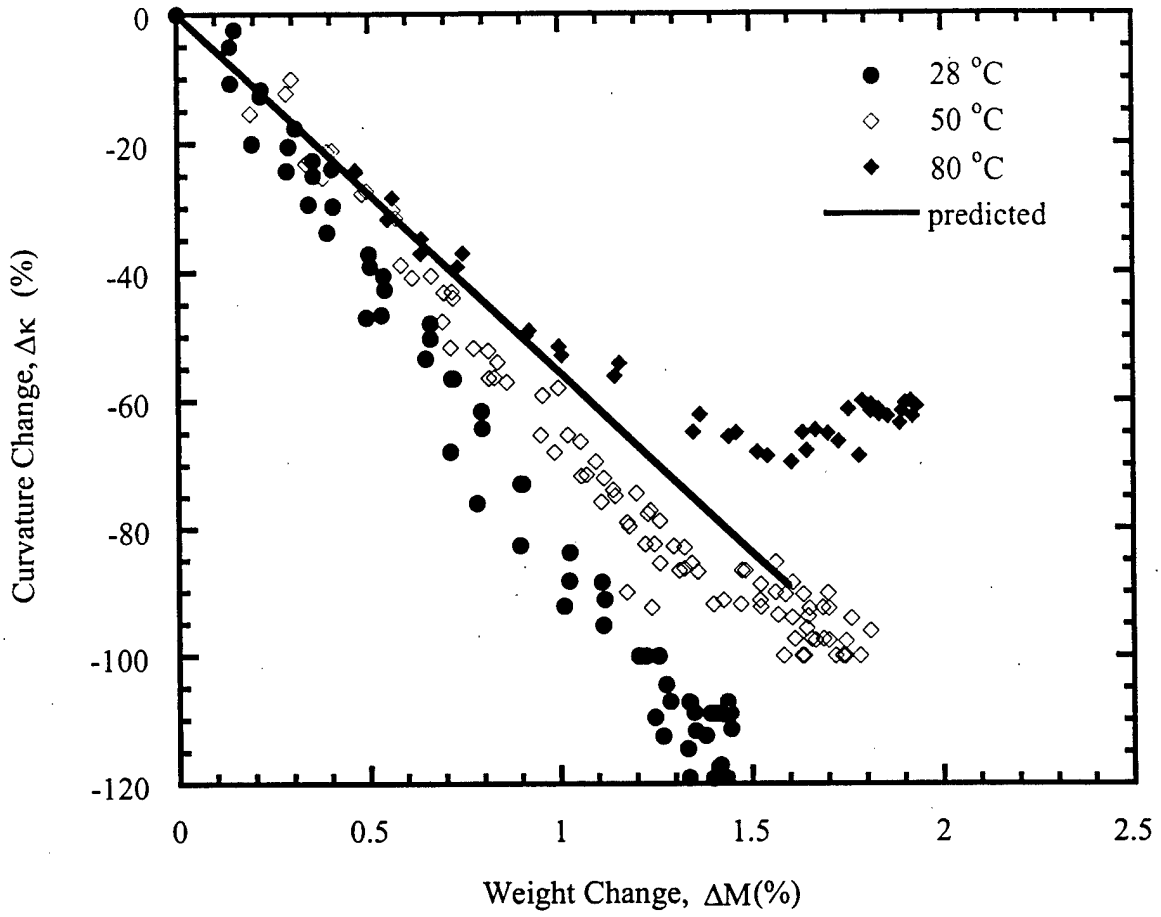

Figure 7 Relationship of curvature and moisture content of laminates in the absorption step. (sample size 150 mm)

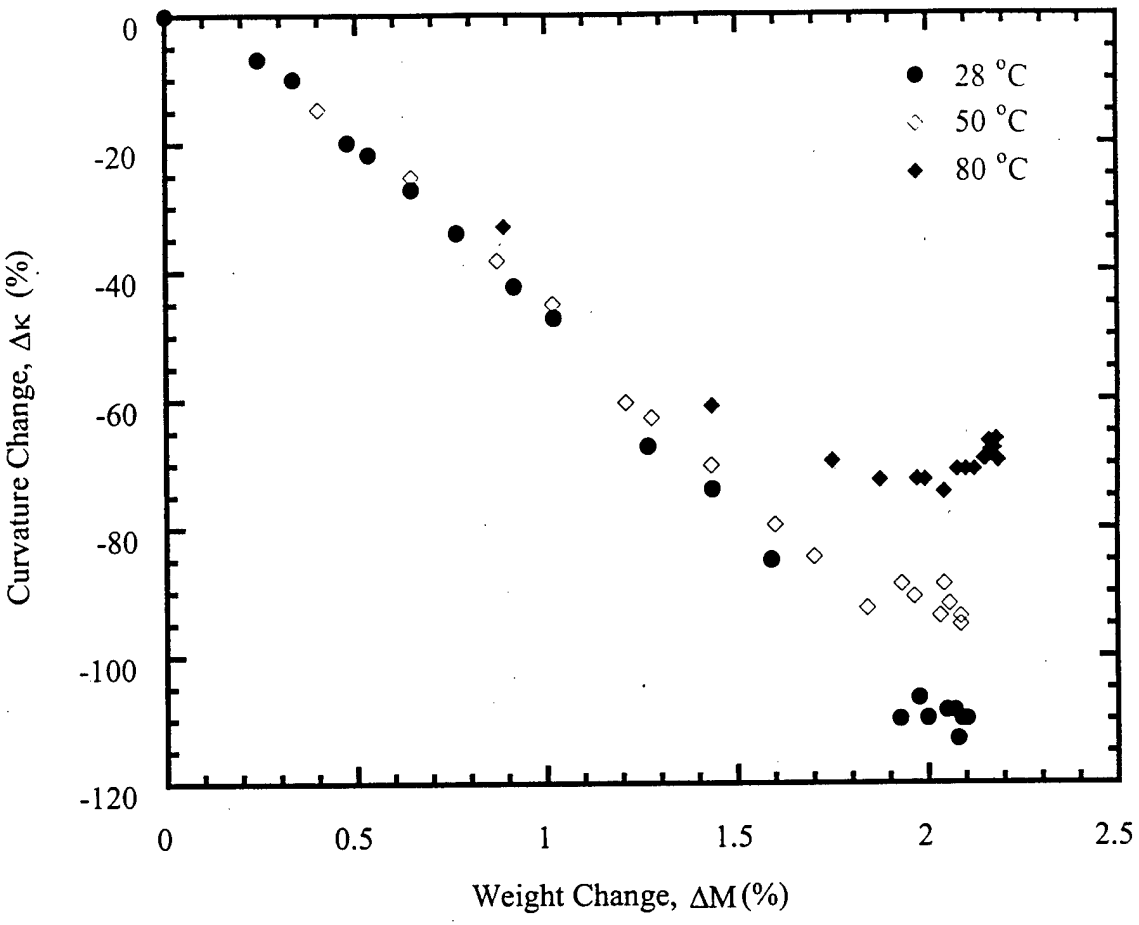

Figure 8 Relationship of curvature and moisture content of laminates in the resorption step where samples were conditioned through a 50 °C absorption and a 80 °C desorption before resorption step (50-80-res). (sample size 150 mm)

INVESTIGATION OF THERMAL DEGRADATION BEHAVIOR OF POLYMERIC COMPOSITES: PREDICTION OF THERMAL CYCLING EFFECTS FROM ISOTHERMAL DATA

INTRODUCTION

In recent years, the drive for material advancements in the aerospace, sporting goods and automobile industries has been increasing steadily. Conventional metals and their alloys are gradually being replaced by new engineering materials such as ceramics and composites based on metals or engineering plastics. Among these new engineering materials, polymeric composites have become more and more important, especially in the field of advanced aircraft applications, where their high strength-to-weight ratio reduces gross weight and as a result, allows an increase in aircraft payloads. Furthermore, it is expected that service life times and maintenance intervals of aircraft will be extended owing to the corrosion and fatigue resistance of polymeric composite materials.

Many of the polymeric resin systems used to build aircraft structures are based on epoxies, bismaleimides, cyanate esters, and phenolics [1]. Epoxies, however, remain the most common resin system for composites used in aircraft structures because they are easily processed and can be prepared with a wide range of properties. Traditionally, polymeric composite systems have been used in aircraft mainly for secondary structures such as control surfaces and interiors. It was not until recent years that components of primary structures such as empennage sections of large commercial aircraft were constructed with composite materials. Considering the overall history of composite materials in the aircraft industry, it may be said that a significant amount of information has been compiled on their material properties. However, the database for composites is not yet sufficient for these materials to be regarded as a reliable replacement for the metals currently used for aircraft primary structures [2].

For example, one of the critical characteristics of aviation materials is their long-term properties under the conditions of aircraft service. In aircraft service conditions, hygrothermal cycling, load cycling, ultraviolet radiation, exposure to jet fuel and hydraulic fluid, as well as paint stripping all affect the stability of composite materials. Virtually all the physical properties of polymericc composites may change with the

passage of time, including structural stiffness, strength, density, deflection due to loading and/or environment, and damage tolerance [3]. As a result, there is a need for a reliable prediction of the maximum lifetime for polymeric composites used in an aircraft service environment. In this respect, practical methods of predicting the long-term durability of composite structures within engineering accuracy must be developed before polymeric composites can be used with confidence in critical load bearing structures.

The goal of the present research is to predict the durability of composites as a function of environmental exposure. More specifically, the present work focuses on the anisotropic effect in the thermo-oxidative degradation behavior of polymer composites under both isothermal and thermal cycling conditions. In this view, it is necessary to make a comprehensive study of the material properties over a wide range of temperatures. In carbon fiber composite systems, the fiber reinforcements have a great influence on the properties of the composite. This observation is explained by the presence of disjoining forces of molecular interactions between polymer molecules and adjacent phases. Additionally, the fibers in the matrices are also known to influence the degradation behavior of polymer composites at elevated temperatures in air environments due to the anisotropy of the composite [4, 5]. Therefore, to investigate the anisotropic effect on thermo-oxidative degradation, weight loss measurements were performed for selected materials in order to quantify the degradation behavior, and to assess the effects of sample size and geometry. Furthermore, the concept of equivalent cycle time (ECT), previously developed to understand the effect of thermal cycling on composite systems, was applied to comprehend the long-term properties of composites, and to shorten the experimental time required to obtain the desired results [6]. Collectively, this work provides an understanding of how the long-term properties of composites are affected, under the controlled environmental conditions, by their inherent characteristics of anisotropy, heterogeneity, and viscoelasticity.

THEORETICAL BACKGROUND

Weight Loss Analyses

Polymers degrade through physical and chemical changes due to reaction of their molecular components with the environment. Among these reactions, oxidation has the largest effect on the properties of the polymer [7]. At normal temperatures, polymers react slowly with oxygen so that oxidation only becomes apparent after a long time. However, oxidative degradation may be induced and accelerated by thermal energy and/or moisture, as well as exposure to radiation. Oxidative degradation in polymeric composites involves solid-gas reactions, and is associated with chain cleavage. As a result, the principal effects of oxidative degradation on polymers are the decay of mechanical properties such as strength, elongation, and resilience, which is a problem common to polymer composites under critical conditions [8, 9]. Experimentally, the rate of oxidative degradation can be determined by measuring the volume of oxygen uptake at a certain temperature. An alternative approach to determine the degradation rate is to measure the weight loss of a polymer specimen, which allows the overall degradation mechanism in polymeric matrices to be obtained.

Previous studies demonstrated that sample geometry affects the degradation behavior of polymers and their composite systems [10] [4]. Moreover, the carbon fibers in composite materials are known to affect the thermal degradation behavior of polymeric composites under elevated temperature in an air environment due to anisotropy [5]. Nam and Seferis considered two different degradation mechanisms of bismaleimide by measuring weight loss with the assumption that either diffusion in the ash layer or chemical reaction by oxygen was rate controlling [4] [11]. In this study, it was assumed that the degradation on each of the sample faces proceeded independently from the surface, and that the degradation on the exposed faces could be added to yield the total weight loss. Later, Salin et al. considered the existence of a bulk degradation mechanism in the early stage of degradation process [12]. Conversely, Cunningham et al. reported using thermogravimetric analysis (TGA) that the weight loss of PMR-15 was solely the result of thermal degradation from the bulk mechanism and that oxygen was not involved in the process [13]. The direct comparison between these results, however, may not be

adequate because the experimental methods and the temperature range used varied in each investigation. Salin et al. studied the degradation isothermally near the glass transition temperature, while Cunningham et al. heated the materials far above the glass transition temperature using dynamic heating methods.

Weight loss can be expressed in various forms that combine initial composite weight (M_0) and transient composite weight (M): normalized weight (M/M_0), extent of weight loss ($\alpha = 1-M/M_0$), and total weight loss ($Q = M_0-M = \alpha M_0$). These expressions are easily converted to one another with the knowledge of the (constant) initial weight. In this study, total weight change was selected to express the weight change of specimen. It is defined as the difference between initial weight and the weight of specimen corresponding to a given stage of the degradation process:

$$Q = M_0 - M \tag{1}$$

where

Q : total weight change (g)

M_0 : initial weight of specimen (g)

M : transient weight of specimen (g)

Considering that the weight change is the result of mass loss from the surface of specimen, total weight loss, Q, can be defined as a summation of the weight loss per unit surface area q_i (g/cm^2) [12] [13]. Then Eq. 1 may be rearranged to give the model suggested in this study to consider the anisotropic degradation of polymeric composites:

$$Q = A_\xi q_\xi + A_\eta q_\eta + A_\zeta q_\zeta \tag{2}$$

where A is the surface area (cm^2). ξ refers to the fiber direction, η normal to the fibers in the transverse direction, and ζ denotes normal to the fibers in the through-thickness direction (to the resin rich surface). The schematic of Figure 1 illustrates the nomenclature used herein. The sample loading axes are referred to as x, y, and z whereas ξ, η, and ζ refer to the fiber axes. For samples where the fiber angle with respect to the surface is either 0° or 90°, the sample and fiber axes coincide.

To account for the direction dependence of weight loss of samples, the following transformations can be used to express the angle dependency of the weight loss fluxes for unidirectional samples that have a fiber angle with respect to the cut surface [4, 12]:

$$q_x = q_\eta \cos^2\theta + q_\xi \sin^2\theta \tag{3.1}$$

$$q_y = q_\eta \sin^2\theta + q_\xi \cos^2\theta \tag{3.2}$$

$$q_z = q_\zeta \tag{3.3}$$

where θ (<90°) is defined as the angle between the sample (loading) axes and the fiber axes.

Unidirectional composite laminates are frequently utilized for research and testing, but most practical applications use more complicated lay-up sequences. Therefore, the diffusion considerations shown here must be extended to cross-ply laminates. The layers with different fiber orientation exposed on a cut surface are in parallel and, consequently, weight loss q_i can be obtained from:

$$q_i = \left(\sum_j A_j q_j \right) / A \tag{4}$$

where the subscript j refers to each layer in the laminate and i to the overall surface. This approach is analogous to the lamination theory, which is used to describe mechanical properties of composite laminates based on properties of individual laminae [14]. The weight loss q_i as a function of fiber angle can be obtained from Eq. 3.1 and Eq. 3.2 in terms of the principal weight loss q_ξ and q_η.

Equivalent cycle time (ECT)

Polymer molecules have a relaxation time which can be long at moderate temperature. Consequently, it is often impractical to obtain real-time measurements of viscoelastic material property changes over long time periods. Nonetheless, the behavior can be readily measured if a variety of temperatures with a fixed time scale is used. This approach is known as time-temperature superposition [7, 15]. Similarly, Prime introduced another descriptive approach based on an Arrhenius expression to explain the degradation

phenomena [16], which was applied to the degree of cure for reacting thermoset systems by Salin et al. [17]. This approach was also applied to dynamic, non-isothermal conditions and viscosity change during cure for polyamide-imide systems [18]. By extending these two methods to composites, equivalent cycle time (ECT) was developed to predict the property changes due to thermal cycling [6].

By definition, equivalent cycle time (ECT) is the characteristic time at a certain isothermal temperature required to have the same extent of material property changes as obtained through thermal cycles. In the case of thermal degradation, ECT can be defined as the time needed at any arbitrary isothermal temperature to obtain the same extent of weight loss as one would through a given number of thermal cycles.

Figure 2 shows a diagram of a thermal cycle and how it may be divided into four segments: isothermal holding (T_l), dynamic heating ($T_l \rightarrow T_m$) with a heating rate β_{lm}, isothermal holding (T_m), and dynamic cooling ($T_m \rightarrow T_l$) with a cooling rate β_{ml}. These four segments repeat in thermal cycles as a function of time.

In order to evaluate the ECT for weight loss, it is necessary first to express the weight loss q as a function of time t. For the purpose, it is convenient to introduce a weight dependent function f(q) which can be determined experimentally:

$$f(q) = D_E t \tag{5}$$

where D_E is an effective diffusion coefficient which can be described by an Arrhenius expression with an activation energy E:

$$D_E = D_{E0} \exp\left(-\frac{E}{RT}\right) \tag{6}$$

where D_{E0} is the pre-exponential factor.

The differential form of Eq. 5 with respect to time t is:

$$\frac{df(q)}{dt} = D_E \tag{7}$$

Under isothermal conditions, Eq. 5 can be directly used with Eq. 6 to evaluate the extent of degradation:

$$f(q) = D_{E0}\exp\left(-\frac{E}{RT}\right)t \tag{8}$$

Eq.8 may be rearranged to give:

$$F(q) = D_{E0}\exp\left(-\frac{E}{RT}\right)\Delta t \tag{9}$$

where

$$F(q)=\left[f(q)\right]_0^q \tag{10}$$

Under dynamic conditions, the heating or cooling rate β is expressed as:

$$\beta = \frac{dT}{dt} \tag{11}$$

Then Eq. 7 can be rearranged and integrated by separation of variables after the application of Eqs. 6 and 11 to give:

$$F(q)=\frac{D_{E0}}{\beta}\int_0^T exp\left(-\frac{E}{RT}\right)dT \tag{12}$$

Eq. 12 is integrated with respect to temperature T and weight loss q to give:

$$F(q)=\frac{D_{E0}E}{\beta R}p(x) \tag{13}$$

where

$$p(x)=\int_\infty^x \frac{exp(-x)}{x^2}dx \tag{14}$$

with $x = E/RT$ (15)

Since p(x) cannot be integrated analytically, a fourth-order polynomial approximation was used in this work to evaluated its values [19]:

$$p(x)=\frac{exp(-x)}{x}\frac{\left(x^3+18x^2+88x+96\right)}{\left(x^4+20x^3+120x^2+240x+120\right)} \tag{16}$$

Weight loss has been expressed using Eq. 9 under isothermal conditions and Eq. 12 under dynamic heating conditions to calculate the ECT of degradation. It is assumed that the degradation reaction mechanism does not change in the temperature range considered so that activation energy E can be considered constant.

To further illustrate the concept of ECT, consider the thermal cycle of Figure 2 and calculate its corresponding ECT at a specified isothermal temperature T_r, which can be referred to as a reference temperature. In order to aid in the calculation, a conceptual diagram representing both the isothermal and the dynamic segments of Figure 2 can be drawn. In Figure 3(a), the isothermal segment is considered. Assuming that the degradation reaction proceeds from q_a to q_b at the isothermal temperature T_l, the time required for this transformation is found to be (t_b-t_a). If the same amount of reaction occurs at the reference isothermal temperature T_r in the period of time Δt_{iso}, Δt_{iso} is defined as an Equivalent Isothermal Time (EIT) at T_r [16]. Similarly, the same concept can be applied to evaluate Δt_{dyn} as an EIT at reference isothermal temperature T_r for the dynamic heating segment shown in Figure 3(b) [6].

Combining the definitions described above with the weight loss functions established in Eq. 9 and Eq. 13, the EITs can be calculated mathematically for both isothermal and dynamic segments. At the isothermal reference temperature T_r shown in Figure 3(a), the extent of weight change from q_a to q_b can be expressed using the weight dependent function:

$$\int_{q_a}^{q_b} f(q)dq = \int_{0}^{q_b} f(q)dq - \int_{0}^{q_a} f(q)dq = F(q_b) - F(q_a) \qquad (17)$$

Then, the extent of weight change may be expressed using Eq. 9 to provide the time required for the progress of reaction at temperature T_r:

$$F(q_b) - F(q_a) = D_{E0}\, exp\left(-\frac{E}{RT_r}\right)\Delta t \qquad (18)$$

When the same extent of reaction occurs at an arbitrary isothermal temperature T_l, Eq. 17 can be rearranged with the introduction of Eq. 9 to give:

$$F(q_b) - F(q_a) = D_{E0}\, exp\left(-\frac{E}{RT_l}\right)(t_b - t_a) \qquad (19)$$

The left-hand sides of Eq. 18 and Eq. 19 are identical. Therefore, the EIT at the reference temperature T_r for an isothermal segment at temperature T_l is:

$$\Delta t = \Delta t_{iso}(T_l) = (t_b - t_a)\, exp\left[\frac{E}{R}\left(\frac{1}{T_r} - \frac{1}{T_l}\right)\right] \qquad (20)$$

When the dynamic segment shown in Figure 3(b) is considered, Eq. 13 can be applied to yield:

$$F(q_b)-F(q_a)=\frac{D_{E0}E}{\beta R}\int_{x_l}^{x_m}\frac{e^{-x}}{x^2}dx$$

$$=\frac{D_{E0}E}{\beta R}\left(\int_{\infty}^{x_m}\frac{e^{-x}}{x^2}dx-\int_{\infty}^{x_l}\frac{e^{-x}}{x^2}dx\right)$$

$$=\frac{D_{E0}E}{\beta R}[p(x_m)-p(x_l)] \qquad (21)$$

Comparing Eq. 21 to Eq. 18, the EIT at T_r can be expressed as follows for the same extent of degradation reaction under the dynamic heating condition considered:

$$\Delta t=\Delta t_{dyn}(T_{lm})=\frac{E}{\beta R}exp\left(\frac{E}{RT_r}\right)[p(x_m)-p(x_l)] \qquad (22)$$

The EIT has been expressed using Eq. 20 and Eq. 22 for isothermal and dynamic segments, respectively. To express the ECT of one thermal cycle, one needs to add the EIT of all isothermal and dynamic segments of the considered cycle. In the case of the thermal cycle of Figure 2, these segments are Δt_{iso} for isothermal holds T_l and T_m, and Δt_{dyn} for dynamic heating β_{lm} and cooling β_{ml}. Then, the ECT at T_r for the total number of the repeated temperature cycles can be shown to be:

$$ECT=\sum_{k}^{N}\left[\Delta t_{iso}(T_l)+\Delta t_{dyn}(T_{lm})+\Delta t_{iso}(T_m)+\Delta t_{dyn}(T_{ml})\right]_k \qquad (23)$$

where N is the total number of thermal cycles applied.

Three Dimensional Consideration

If Eq. 23 is extended to express the degradation of anisotropic materials, each weight loss expression (q_i) in the ξ, η, and ζ directions needs to be considered separately to get Δt_{iso} and Δt_{dyn} for ξ, η, or ζ.

Under isothermal conditions:

$$F(q_i)=D_{E0,i}exp\left(-\frac{E_i}{RT}\right)\Delta t \qquad (24)$$

Under dynamic conditions:

$$F(q_i) = \frac{D_{E0,i} E_i}{\beta R} p(x_i) \tag{25}$$

Then the ECT expression for a three-dimensional anisotropic degradation and a total number N of thermal cycles is:

$$ECT_i = \sum_{k}^{N} \left[\Delta t_{iso,i}(T_l) + \Delta t_{dyn,i}(T_{lm}) + \Delta t_{iso,i}(T_m) + \Delta t_{dyn,i}(T_{ml}) \right]_k \tag{26}$$

where i represents ξ, η, or ζ.

The reference temperature, T_r, can be any temperature of interest, and only the knowledge of the activation energy E is required to calculate the ECT.

EXPERIMENTAL

A unidirectional carbon fiber reinforced epoxy composite was selected for this study. The material was a high performance system currently used by the aircraft industry to make both laminates and honeycomb structures. This high performance prepreg, known as F593, consisted of a rubber-modified epoxy with T-300 carbon fibers, and was manufactured by Hexcel Corporation. The F593 resin system is self-adhesive and provides excellent laminate and honeycomb sandwich properties. The resin content of the prepreg used in this study was found to be 37.6% by a solvent extraction method [Boeing, 1992 #75].

The prepreg was compacted and cured at 177°C for 90 minutes according to the manufacturer's recommendation. Three types of laminates were prepared for weight loss measurements: a unidirectional 26-ply laminate, a unidirectional 14-ply laminate, and a $[0/90]_{13S}/0$ 27-ply laminate consisting of cross-ply layers with 0/90° fiber angles. Samples were cut into rectangular shapes from the cured laminates using a diamond saw, and cut surfaces were polished to provide uniform, smooth surfaces using first 120 grit sandpaper and finally 320 grit sandpaper. After the cut surfaces were polished, samples were cleaned with methanol and dried at 80 °C for three days to eliminate possible volatile residues or moisture in the sample matrices.

Eleven samples with different geometry were prepared by varying dimensional size and fiber orientation to observe the weight loss in the x, y, and z directions. In order to determine the effect of geometry on weight loss, unidirectional laminates were cut to

position the fibers at four different angles. Table 1 shows the sample geometry and notation used throughout this study.

Samples were divided in five groups and were evaluated for thermo-oxidative degradation under atmospheric conditions. Four groups were tested isothermally at temperatures of 170°C, 180°C, 190°C, and 200°C, while the fifth group was put into a Lindberg tube furnace and thermally cycled from 80°C to 200°C. The detailed description of the thermal cycles used in these experiments is provided in the Results and Discussion section. Samples were periodically weighed to within 0.0001 gram precison with a Sartorius electronic balance.

Dynamic mechanical tests were performed to evaluate the thermo-mechanical property changes at both 190°C and 200°C as a function of time for C1 type specimens with a TA Instrument DMA 983 apparatus coupled to a TA Instruments 2100 Thermal Analyzer for data acquisition and reduction. The heating rate was 5°C/min from room temperature to 250°C, and the oscillation amplitude was set to 0.1 mm. Nitrogen gas was used with a flow rate of 300 ml/min during all DMA experiments.

To observe specimen morphology changes, cross-sections of specimen were prepared and examined by microscope.

RESULTS AND DISCUSSION

Isothermal Degradation

The weight loss data for both the unidirectional and cross-ply samples were collected at various temperatures and analyzed anisotropically to obtain weight loss values for each individual surface at various temperatures.

Figure 4 shows the results of weight change (%) as a function of time at 170°C, 180°C, 190°C, and 200°C for both A and B type specimens which are unidirectional samples. In these samples, the number 1 refers to specimens that have the fibers running in the longitudinal direction, while number 2 refers to specimens that have the fibers running in the transverse direction. From the data in Figure 4, it was found that the weight dropped rapidly and then leveled off and approached a constant value as time increased. For each type of specimen, the weight loss rate was found to be higher at higher temperatures. It should be noted that the difference was hardly observed among

the samples during the initial stage of weight loss. This initial surface area independent degradation might have resulted from degassing of low molecular weight components created by chain cleavage in the matrices. One important thing to mention, however, is that the matrix of the specimens used in this study was a rubber modified system. Therefore, the major initial weight loss could have resulted from the degradation of the rubber structure in the matrix. As degradation proceeded with time, the weight loss rate of each sample varied depending on sample geometry, showing anisotropic degradation behavior. It was found that the higher the surface to volume ratio of the specimen, the faster the weight loss rate. Interestingly, the weight loss rate was not significantly affected by fiber orientation. It was expected that the specimens denoted by the number 2 (fiber in the transverse direction) would have a greater weight loss rate than those denoted by the number 1 (fibers in the longitudinal direction) because of the high thermal conductivity of the fibers and the fact that the number 2 specimens had a larger surface area normal to the fiber direction [12]. From the results of Figure 4, it is suggested that the fiber direction might not be the major factor affecting the weight loss rate in the present experiments.

Figure 5 shows the evolution of the glass transition temperature (T_g) during weight loss experiments at 190°C and 200°C. It was found that the glass transition temperature dropped dramatically in the initial stage of weight loss. In case of aging at 200°C, the glass transition temperature dropped from 187°C to 167°C after 7 hours. It is interesting to note that the weight loss was less than 0.3% at this stage. After the initial drop, the glass transition temperature continued to decrease slightly until 350 hours had elapsed, where the corresponding weight loss was 1.3%. After 350 hours, the glass transition temperature was found to increase slightly. In case of aging at 190°C, the glass transition temperature dropped from its initial value of 187°C down to 165°C after 50 hours. In both temperatures, it may be assumed that weight loss was mainly characterized by the degradation of the rubber modifier, leading to a dramatic reduction in the T_g of the material in the initial stage. After that, the rubber modifier kept degrading, hence the T_g kept decreasing. In these stages, the degradation of the rubber modifier dominated the decrease in T_g; while the additional cross-linking in the matrix resin material served to increase the T_g. After depletion of the rubber modifier the matrix

may have become brittle, increasing the T_g somewhat as time elapsed due to the degradation as well as additional cross-linking. It was found from Figure 5 that samples having undergone the same weight loss but at different temperatures (i.e. 190°C vs. 200°C) did not have the same T_g. This implied that weight loss may not be most relevant descriptor to predict mechanical property changes [20].

Weight Loss Modeling

The weight loss behavior of the specimens presented in this study was modeled considering surface dependent oxidative degradation based on the shrinking core model [4] [12].

$$q_i = D_{Ei} t^{n_i} \tag{27}$$

where the subscript i refers to either ξ, η, or ζ, n_i is a time exponential factor, and D_{Ei} is an effective diffusion coefficient that may be described by an Arrhenius expression with activation energy E. If the weight loss is limited by the diffusion, then value of n_i will show 0.5; if it is limited by the reaction kinetics, n_i will be 1. If the rate is not limited by a single step, the experimentally determined constant $D_{E,i}$ is for both the thermal degradation reaction and diffusion.

Calculations were made to obtain geometry dependent q_i's which were intrinsic terms that resulted from the anisotropic oxidative degradation of six samples (samples No.1 to No.6 in the first column of Table 1). A matrix solving method was developed and applied to the weight loss data in order to evaluate the three unknown weight losses per unit surface area in the x, y, and z directions. While calculating these values, it was found necessary to introduce an extrinsic term that expressed weight loss due to thermal degradation which was not dependent on oxygen diffusion. Therefore, Eq. 2 was modified to consider an extrinsic term q_ζ':

$$Q = A_\xi q_\xi + A_\eta q_\eta + A_\zeta (q_\zeta + \kappa q_\zeta') \tag{28}$$

where κ is a modeling parameter representing a dimensionless characteristic diffusion length, and

$$q_\zeta' = D_{E\zeta}' t / (D_{E\zeta}' t + 1) \tag{29}$$

with effective diffusion coefficient $D_{E\zeta}$'.

Evaluation of these model parameters was carried out using Eqs. 27 to 29 in a spreadsheet software with the assumption that q_η had the same value as q_ξ. This assumption was reasonable considering that the η and ζ directions (transverse and through-thickness) were both perpendicular to the fibers direction and therefore were in a quasi-isotropic conformation.

Table 2 summarizes the final results obtained by the inclusion of this extrinsic term. The time exponents obtained for ξ and η (and ζ) direction were found to have different values, implying that the mechanism of oxidation was anisotropic. Despite the fact that all three time exponents differed, they were found to remain close to the value of 0.5, indicating that degradation was governed by an anisotropic diffusion controlled mechanism. Eq. 29, applied on the extrinsic term, was found to be in good agreement with the data as will be shown later.

Figure 6 shows the comparison between the calculated values from the model using the parameters in Table 2 and the experimental data set of (a) A1 and (b) B2 at 170°C, 180°C, 190°C and 200°C, respectively. In these samples, the fiber direction ξ corresponds also to the longitudinal direction of specimen x. It is seen from these figures that the proposed model described the data adequately over the entire temperature range.

In addition to unidirectional specimens with $\theta = 0°$ or 90°, weight losses of specimens with intermediate values of θ were predicted using Eqs. 3.1 through 3.3. Comparison of data and predictions for C-type samples at 180°C are shown in Figure 7 to illustrate the effect of fiber angle, where the fiber angle of C3-type specimen is 30° with respect to x axis. The model matched the data well for three different type specimens. In the case of the data at 190°C and 200°C, slight discrepancies were found between the data and model prediction. These observations may be explained by the faster rate of degradation of the rubber at high temperatures, leading to an earlier depletion of the rubber phase.

Weight loss of cross-ply specimens were predicted using Eq. 6 [12], where number 5 means cross-ply. Agreement between the data and model predictions at 180°C are displayed in Figure 8(a). Figure 8(b) shows the data set of A5 at 170°C, 180°C, 190°C and 200°C. Small deviations between predicted values and the experimental data were observed at 190°C and 200°C with the same reason as mentioned in the case of Figure 6.

Collectively, as seen in Figures 6 to 8, the proposed model matched the data successfully, and adequately expressed the anisotropic degradation of carbon fiber composites over the entire experimental temperature range.

Temperature Cycling Considerations

The thermal cycling effect on weight loss of polymeric composite laminate was investigated, and the ECT concept developed above was applied to predict the weight loss behavior under the thermal cycles using isothermal weight loss data [6]. A schematic of a thermal cycle was shown in Figure 2. Conditions used in this study consisted of a two hour hold at 80°C (T_I), heating at 5.27°C/min to 196°C ($T_I \rightarrow T_m$), a two hour hold at 196°C (T_m), and cooling at 1.05°C/min to 80°C ($T_m \rightarrow T_I$).

Figure 9 shows the weight losses for samples A1, B1, C1 as a function of the number of cycles. Weight loss obtained through cycling was similar to that of isothermal experiments, i.e. a sharp initial drop in weight, followed by an asymptotic behavior. As indicated by Eq. 20 and Eq. 22, the parameter required for the calculation of the equivalent cycle time is the activation energy of each reaction involved. The activation energies (kJ/mol) were evaluated from the slopes of the lines (for these samples ξ coincided with x) using the Arrhenius equation, and summarized in Table 3.

ECTs were calculated for q_i (q_x q_y, q_z) and q_z' using Eq. 20 and 22 [6]. Each EIT calculated for each isothermal and dynamic segment was added to evaluate the ECT corresponding to one thermal cycle. The reference temperature T_r was selected as being 196°C, which was the second isothermal holding temperature in the thermal cycle used in this study. Results of the calculated ECTs for q_i and q_z' for one temperature cycle are listed along with activation energies in Table 3, where the equivalent isothermal times (EITs) at each segment (two isothermal holding, one dynamic heating, and one dynamic cooling) are also summarized. The EIT of the 80°C isothermal segment was found to be negligible for each reaction. It was also interesting to notice that the equivalent cycle time was different in each direction, bringing insights to the anisotropic behavior of composites during degradation.

The ECTs calculated here for four different weight loss reactions were converted into the number of cycles, and the thermal cycle effect on weight loss could be

determined by using Eq. 26 with the relevant parameters. Figure 10 shows the computed weight loss along with the experimental data of samples A1, B1, and C1. As can be seen in the figure, the weight loss predicted using the isothermal weight loss data was found to be in good agreement with the experimental data for the specimens examined. It was found that the predicted values slightly deviated from the experimental data after the initial stage of weight loss. This implies that the degradation process of composite materials might be accelerated by physical property changes in the matrix due to thermal cycles. Compared to the weight loss in isothermal conditions, one of the main differences could be the formation and growth of invisible microcracks caused by the thermal cycles. These microcracks could possibly provide additional diffusion paths for the degradation products, and explain why these products could diffuse out of the sample surfaces more rapidly.

PHYSICAL OBSERVATION BY MICROSCOPY

Cross sections of the specimens were subsequently prepared and examined by optical microscopy. Figure 11 shows photomicrographs at 20X magnification of the specimens that were (a) unaged and (b) aged through thermal cycles. Contrary to the expectation from the discussion centered around Figure 10, no visible voids or microcracks were found in the matrices of any of the specimens. Cracks moving inward from the surfaces were found in the first layers of the specimen shown in Figure 11(b), but could not be found in the interior of the matrix. Nonetheless, these small cracks may have contributed to increasing the diffusion rate of the degradation products when they reached close to the surface. It cannot be ruled out that the resin matrix contained microcracks or other features such as voids which were not detectable by conventional techniques, or might have been weakened or obscured during sample preparation.

CONCLUSIONS

In this study, experiments were conducted to evaluate the degradation properties of carbon fiber/epoxy composite materials through weight loss measurements.

In isothermal experiments, it was found that the weight loss of each sample varied according to sample geometry, indicating that degradation was an anisotropic phenomenon. It was found that the higher the surface to volume ratio of a specimen, the more weight loss it suffered. Next, a model was developed to predict the overall degradation. The proposed model took into account the anisotropic behavior of the material, and contained an intrinsic and an extrinsic diffusion term. Model predictions were found to match the experimental data successfully, and they accurately expressed the anisotropic degradation effect over the entire experimental temperature range.

Finally, the determination of the equivalent cycle time (ECT) of the material was undertaken. The parameters required to predict the thermal cycling effect on material degradation were evaluated using isothermal experimental results. The resulting prediction was found to be in good agreement with the experimental data for all specimens investigated here, and proved to be an effective technique for the evaluation of long-term thermal degradation behavior by thermal cycling.

REFERENCES

1. Williams, J.G., Resin Systems, New York: American Institute of Aeronautics and Astronautics, Inc., (1986).
2. Seferis, J.C., S. Zeng, A.G. Miller, D.S. Krebs, and C. Blohm, Proc. of National Academy of Athens, 1-12 (1999).
3. Progelhof, R.C. and J.L., Throne Polymer Engineering Principles, Cincinnati: Hanser/Gardner Publications, Inc., (1993).
4. Nam, J.D. and J.C. Seferis, SAMPE Quarterly, **24** 10-18 (1992).
5. Tanaeva, S.A., L.V. Bulgakova, L.S. Domorod, and L.E. Evseeva, Inzhennerno-Fizicheskii Zhurnal, **29** 1057-1062 (1975).
6. Chung, K., J.C. Seferis, and J.D. Nam, Proceedings of the Thirties Annual Technical Meeting of the Internaltional Metallograpic Society, **25** 247-251 (1997).
7. Krevelen, V., Properties of Polymers, Elsevier, (1990).
8. Meyer, M.R., R.J. Friedman, H.D.J. Schutte, and L.R.A. Jr., Journal of Biochemical Materials Research, **28** 1221-1231 (1994).
9. Li, Y., B. Gao, and J. Unsworth, Proceedings of the 4th Internaltional Conference on Properties and Applications of Dielectric Materials, 752-755 (1994).
10. Bowles, K.J., G. Nowak, and T.A. Leonhardt, SAMPE Quarterly, **24** 3-9 (1993).
11. Seferis, J.C. and J.D. Nam, Proc. of National Academy of Athens, 100-123 (1992).
12. Salin, I.M. and J.C. Seferis, Polymer Composites, **17** 430-442 (1996).
13. Cunningham, R.A., S.M. Candidate, and H.L. McManus, Grant NAGR 1760, March (1996).
14. Mallick, P.K., Fiber-Reinforced Composites, New York: Marcel Dekker, Inc., (1993).
15. Ward, I.M, Mechanical Properties of Solid Polymers, John Wiley & Sons, (1983).
16. Prime, R.B., Proceeding of the 14th North American Thermal Analysis Society Conference, 137-144 (1985).

17. Salin, I.M., J.C. Seferis, C.L. Loechelt, and Rothschilds, SAMPE Quarterly, 154-63 (1992).

18. Copeland, S.D., J.C. Seferis, and M. Carrega, J. Appl. Polym. Sci., **44** 41-53 (1992).

19. Senum, G.i. and R.T. Yang, J. Thermal. Anal., **11** 445-447 (1977).

20. Bowles, K.J., SAMPE Quarterly, 2-11 (1992).

Table 1 Sample geometry and identification

No.	I.D.	Dimension (mm)			θ between ξ and x (°)	S/V (cm^{-1})
		x	y	z		
1	A1	41	21	4.06	0	6.4
2	A2	41	21	4.06	90	6.4
3	B1	41	12	4.06	0	7.1
4	B2	41	12	4.06	90	7.1
5	C1	41	6	4.06	0	8.7
6	C2	41	6	4.06	90	8.7
7	C3	41	6	4.06	30	8.7
8	A5	41	21	4.2		6.2
9	B5	41	12	4.2	Cross-ply	6.0
10	C5	41	6	4.2		8.6
11	G5	20	6	4.2		9.1

Table 2 Summary of model parameters.

	170°C	180°C	190°C	200°C
n_x	0.5	0.5	0.5	0.5
n_y	0.7	0.7	0.7	0.7
n_z	0.7	0.7	0.7	0.7
D_x	2.03×10^{-5}	3.20×10^{-5}	4.04×10^{-5}	6.93×10^{-5}
D_y	1.93×10^{-6}	2.60×10^{-6}	1.09×10^{-5}	2.85×10^{-5}
D_z	1.93×10^{-6}	2.60×10^{-6}	1.09×10^{-5}	2.85×10^{-5}
κ	0.01787	0.0181	0.01765	0.0171
D_z'	0.00259	0.00677	0.01589	0.02770

Table 3 Calculated EIT and ECT for one cycle of Figure 2.

	Anisotropic parameter direction			
	ξ	η	ζ	ζ'
EIT for segment 1 [80°C, 120 min]	0.00123	2.8×10^{-7}	2.8×10^{-7}	0.00098
EIT for segment 2 [80°C→196°C, 22 min]	2.4126	1.4239	1.4239	2.3676
EIT for segment 3 [196C, 120°C min]	120	120	120	120
EIT for segment 4 [196°C→80°C, 110 min]	12.0629	7.1194	7.1194	11.8381
ECT	134.48	128.54	128.54	134.21
E (kJ/mol)	136.4	236.2	236.2	139.1

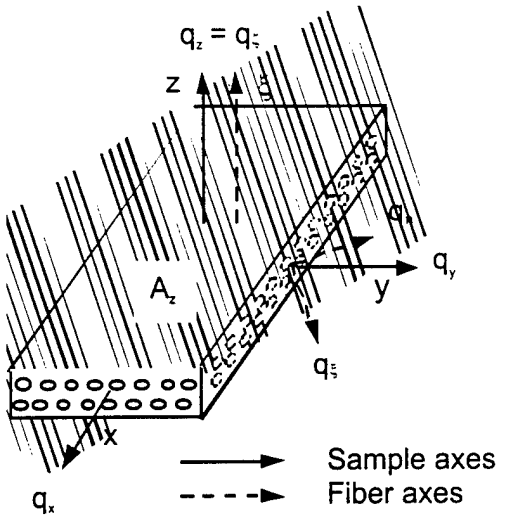

Figure 1 Sample geometry and axes definition.

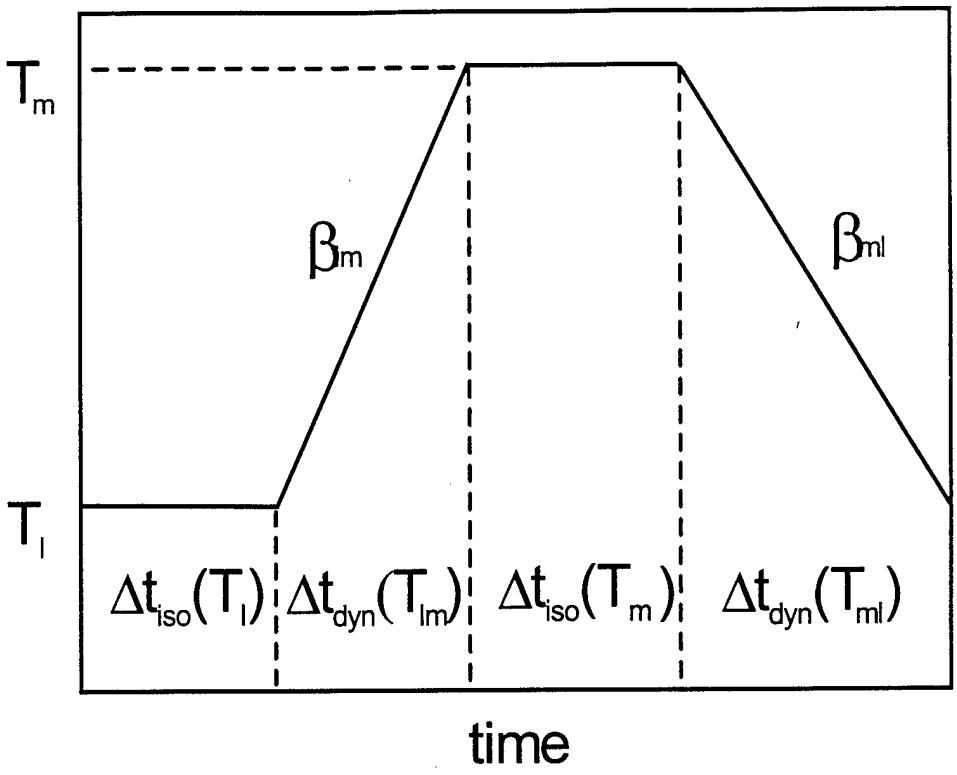

Figure 2 Schematic diagram of a thermal cycle containing two isothermal holds and two dynamic heating/cooling segments.

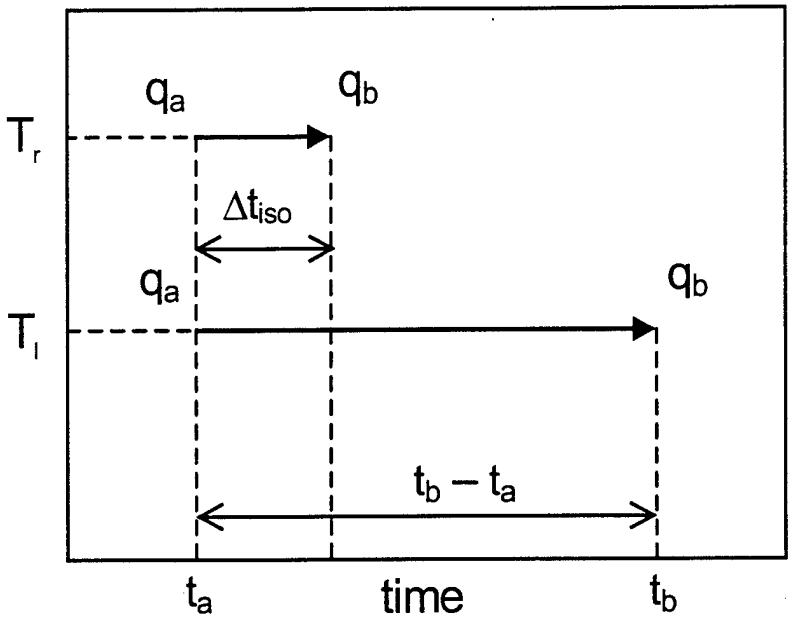

Figure 3(a)

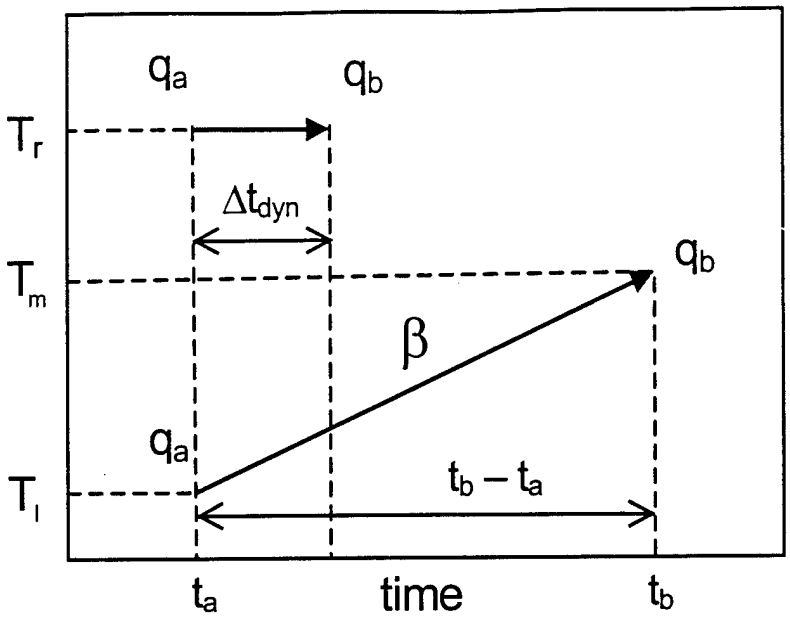

Figure 3(b)

Figure 3 Conceptual diagram of equivalent isothermal time and equivalent cycle time (a) Isothermal segment (b) dynamic segment.

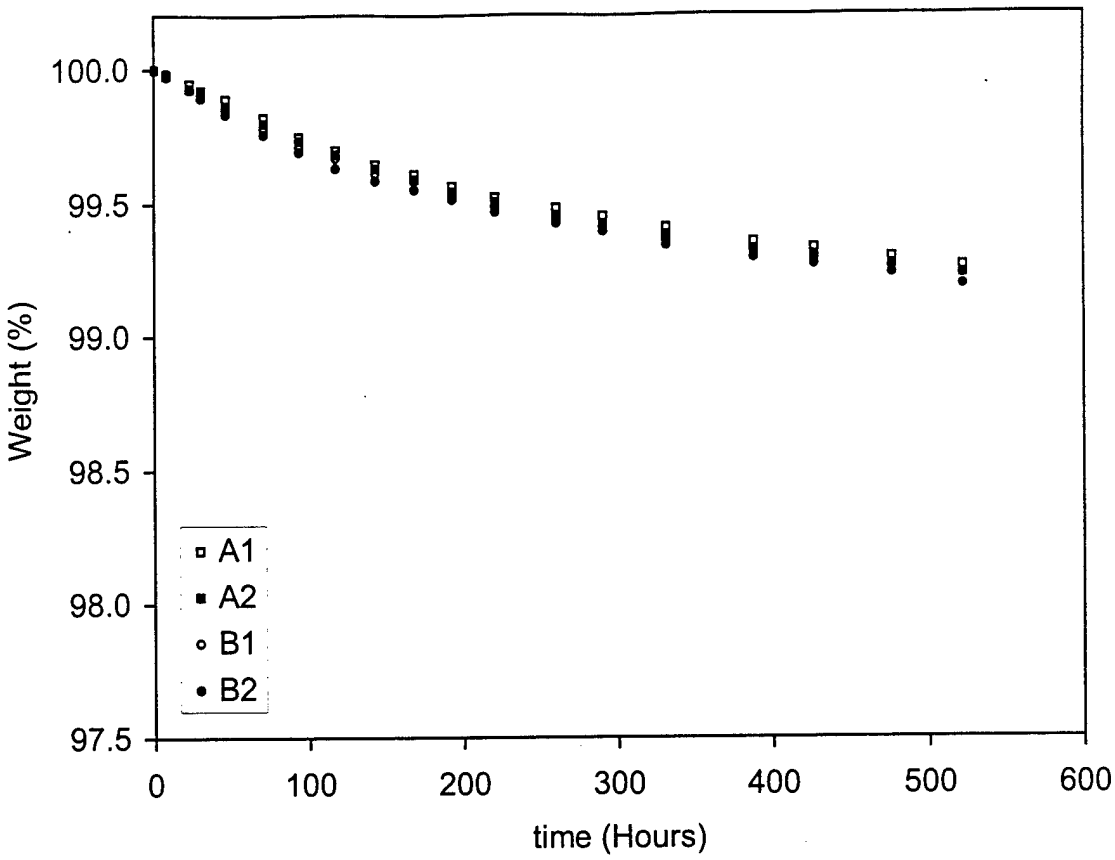

Figure 4(a) Effect of specimen size and fiber direction on sample weight change at (a) 170°C (b) 180°C (c) 190°C (d) 200°C.

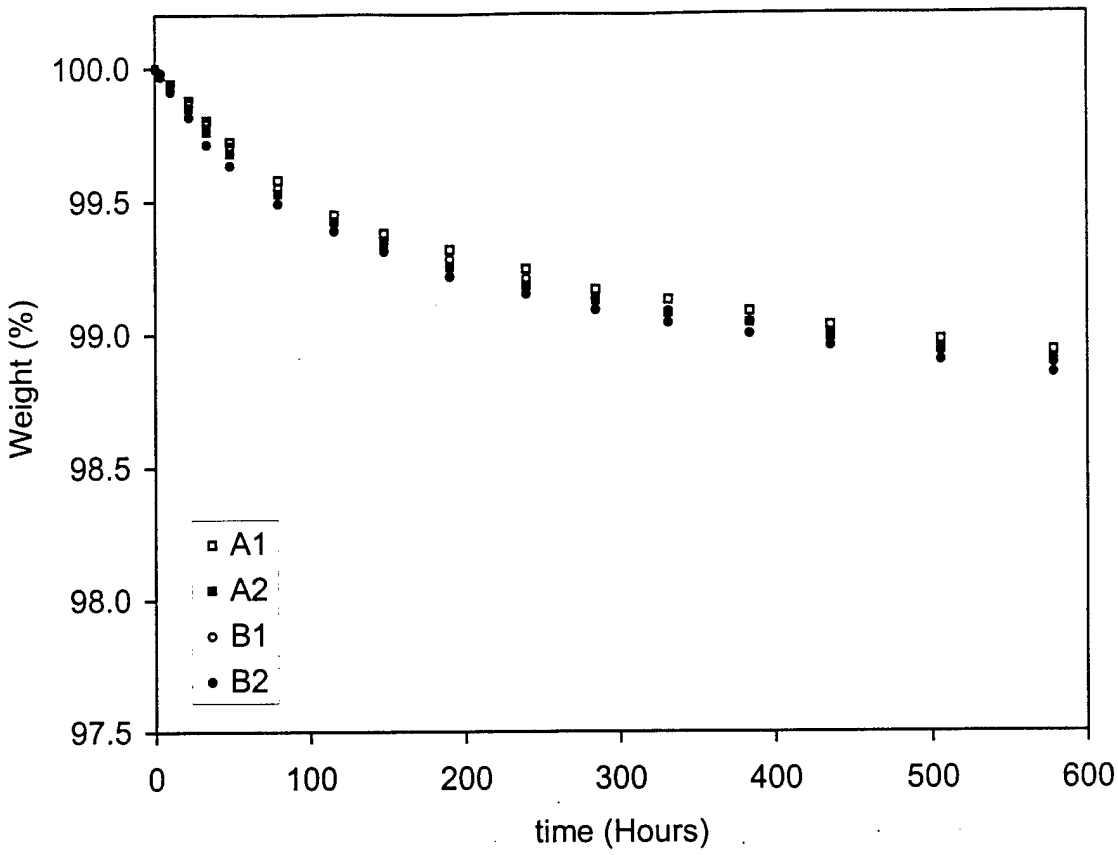

Figure 4(b) Effect of specimen size and fiber direction on sample weight change at (a) 170°C (b) 180°C (c) 190°C (d) 200°C.

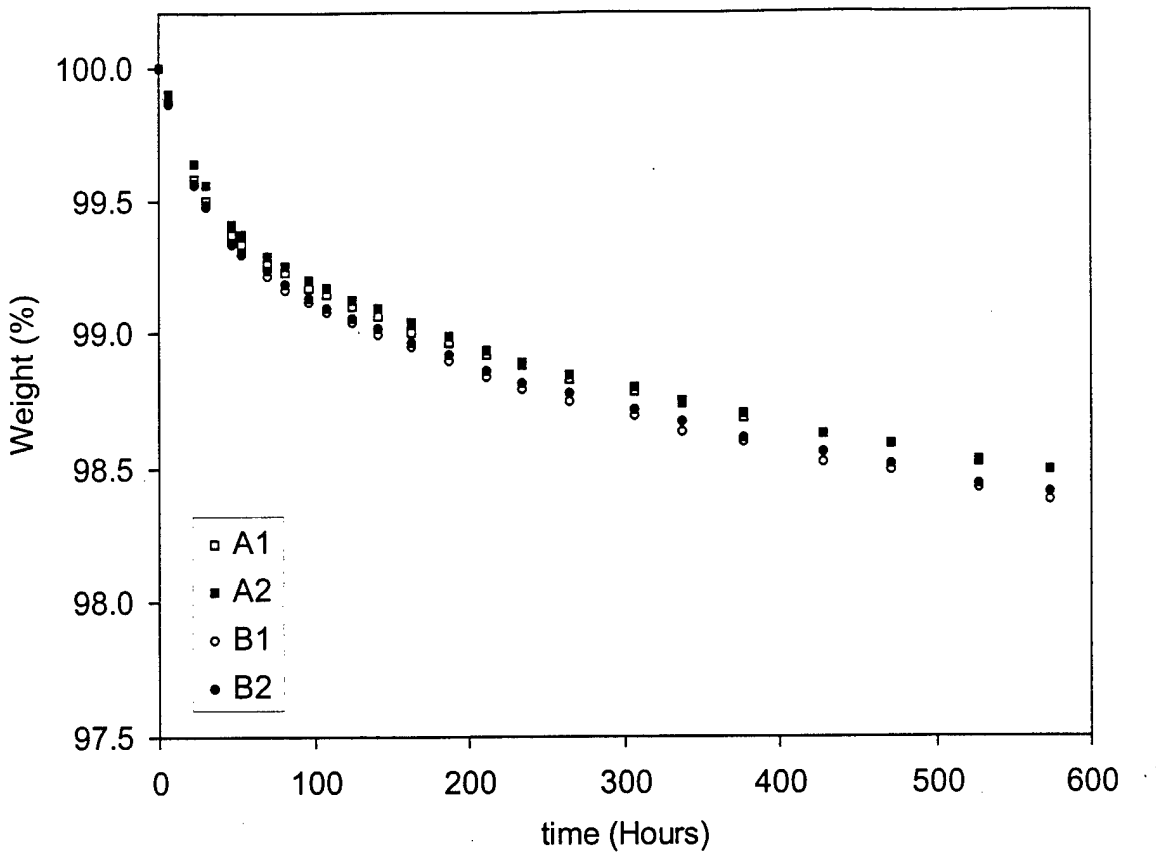

Figure 4(c) Effect of specimen size and fiber direction on sample weight change at (a) 170°C (b) 180°C (c) 190°C (d) 200°C.

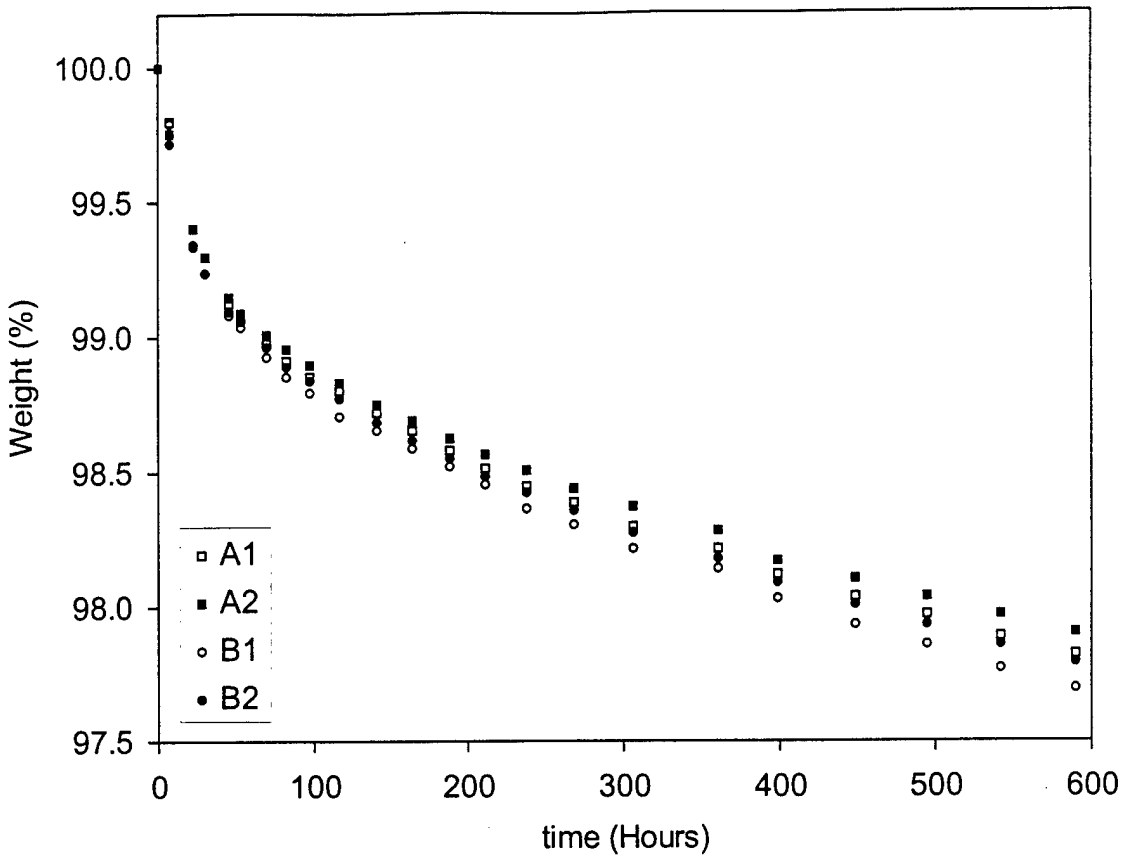

Figure 4(d) Effect of specimen size and fiber direction on sample weight change at (a) 170°C (b) 180°C (c) 190°C (d) 200°C.

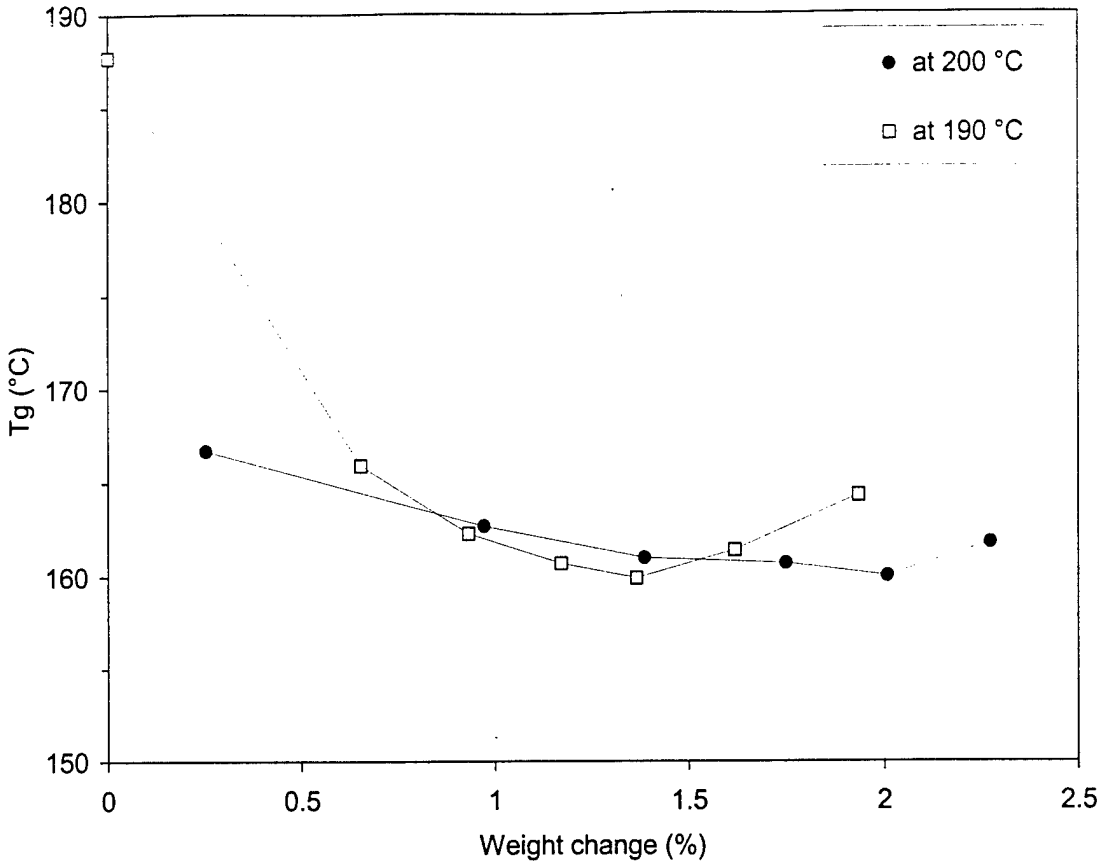

Figure 5 Evolution of the glass transition temperature as a function of time. T_g was determined by DMA.

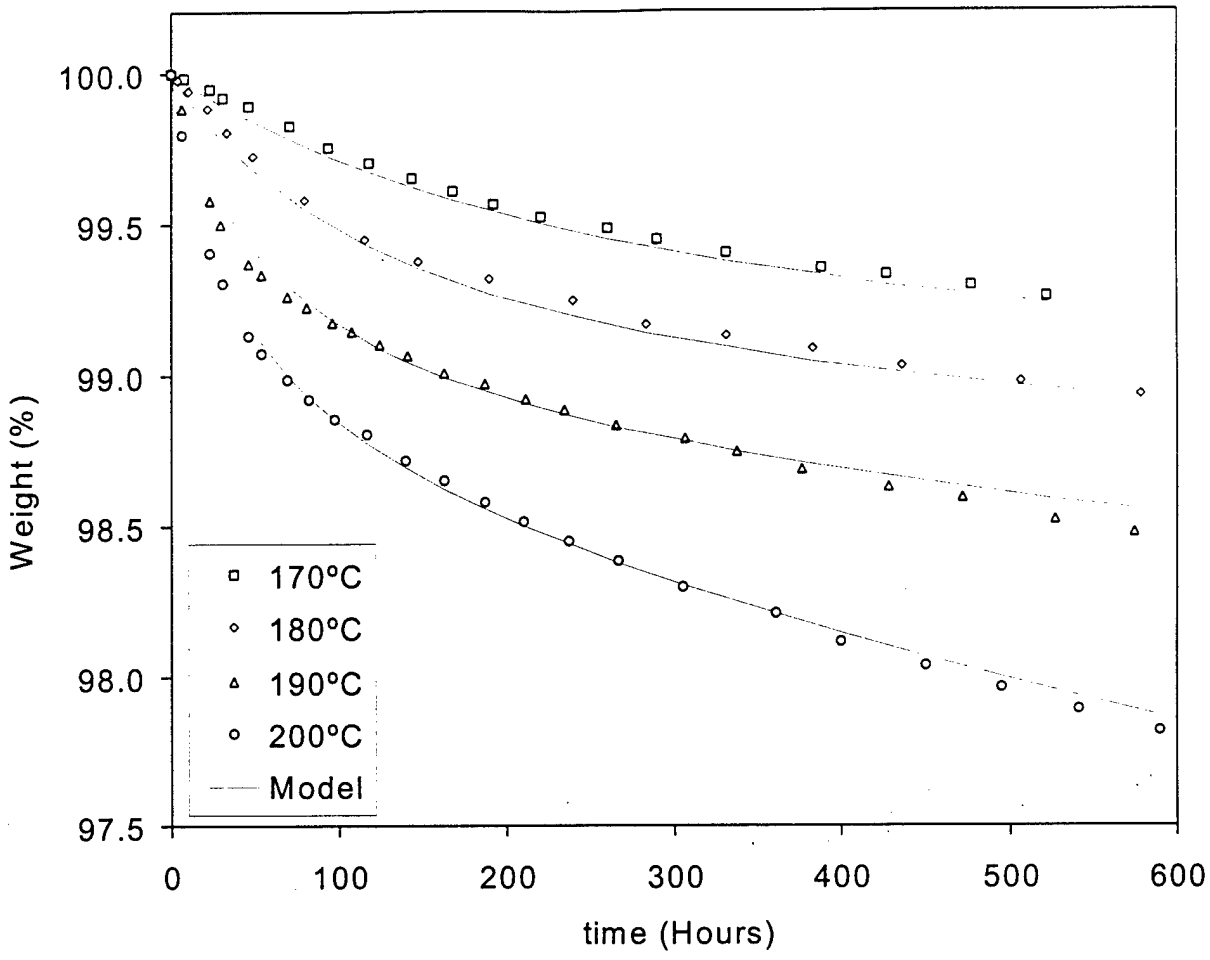

Figure 6(a) Experimental data vs. model prediction for (a) A1-type specimens (b) B2-type specimens at 170°C, 180°C, 190°C, and 200°C, respectively.

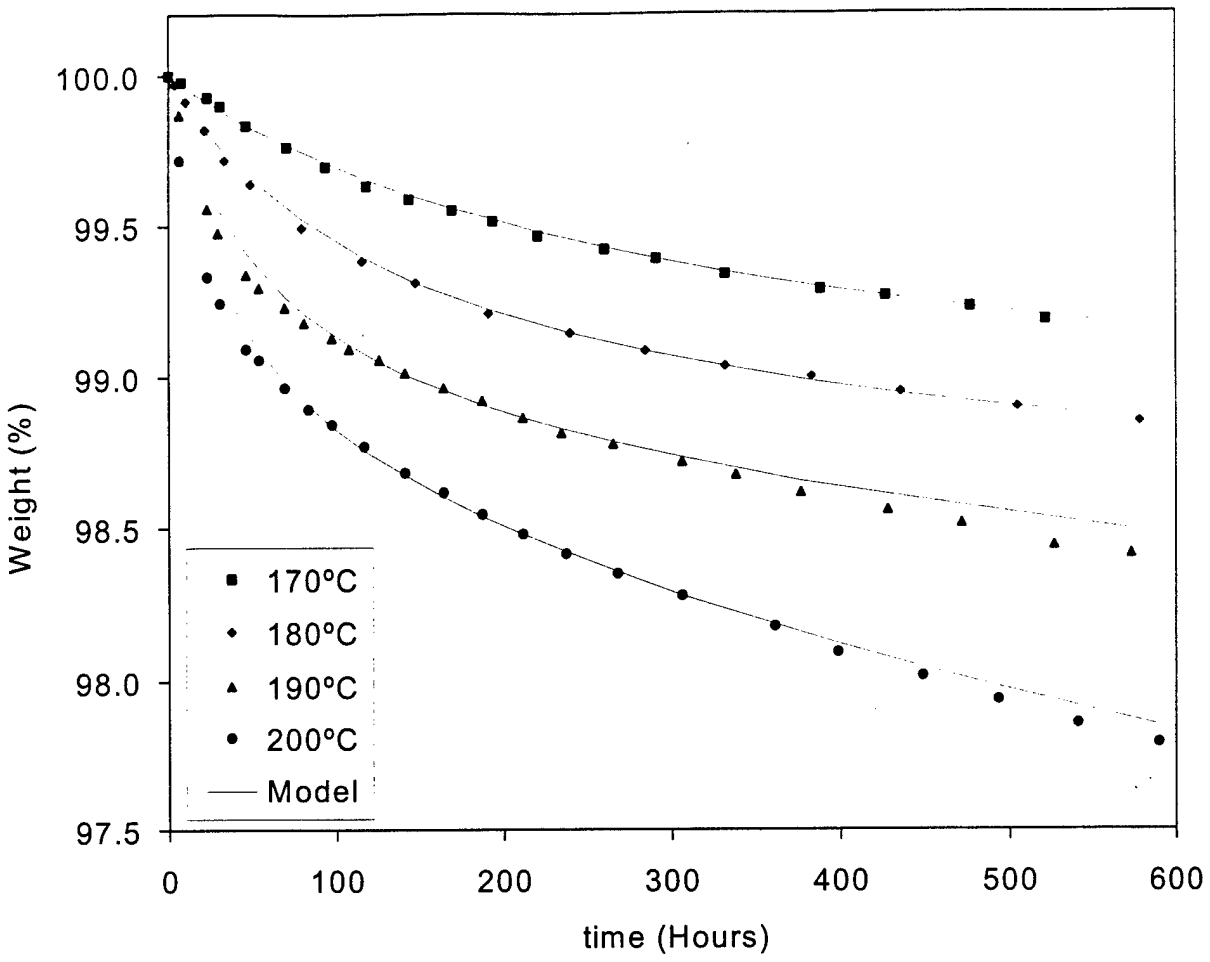

Figure 6(b) Experimental data vs. model prediction for (a) A1-type specimens (b) B2-type specimens at 170°C, 180°C, 190°C, and 200°C, respectively.

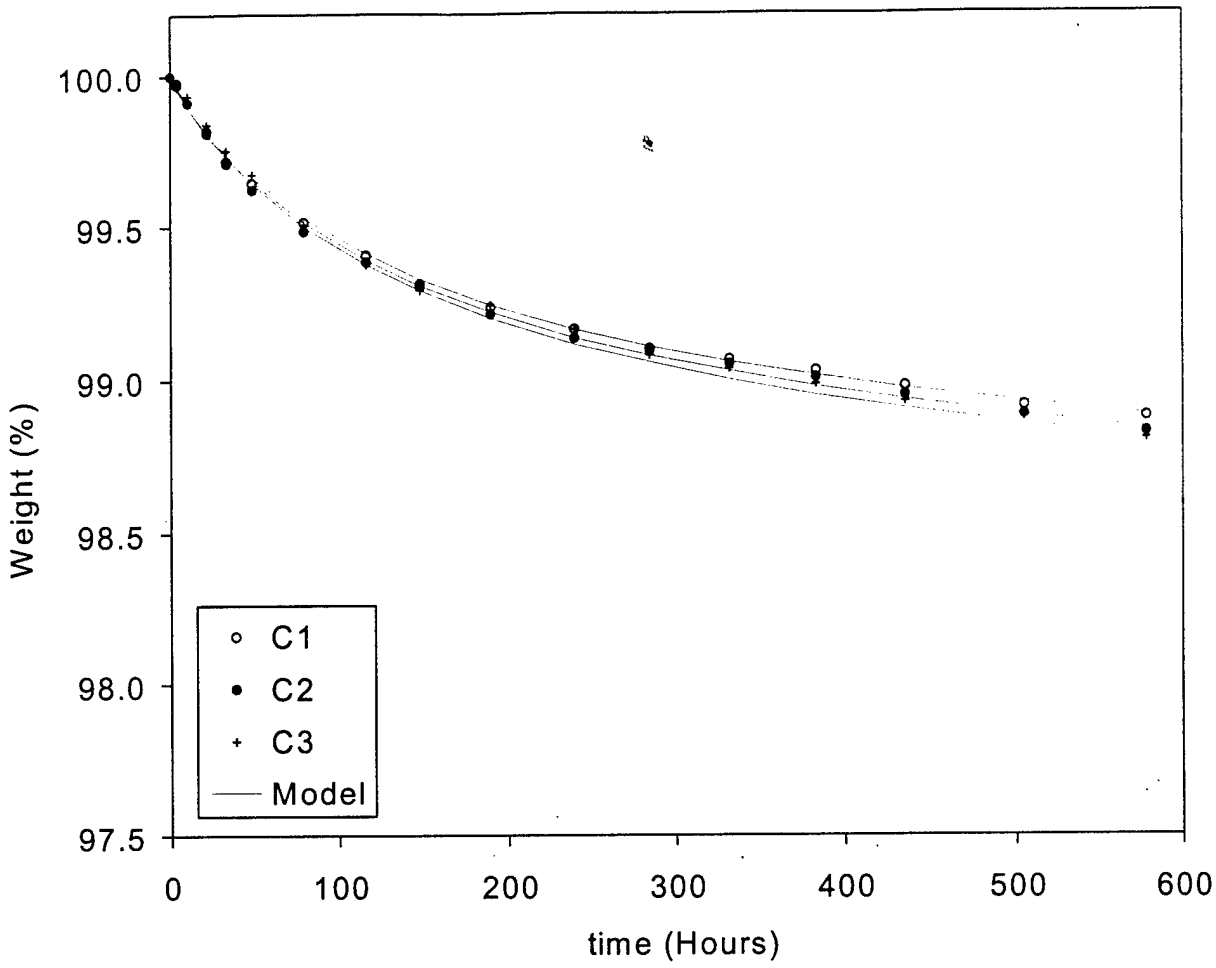

Figure 7 Data vs. model prediction for various fiber orientations at 180°C.

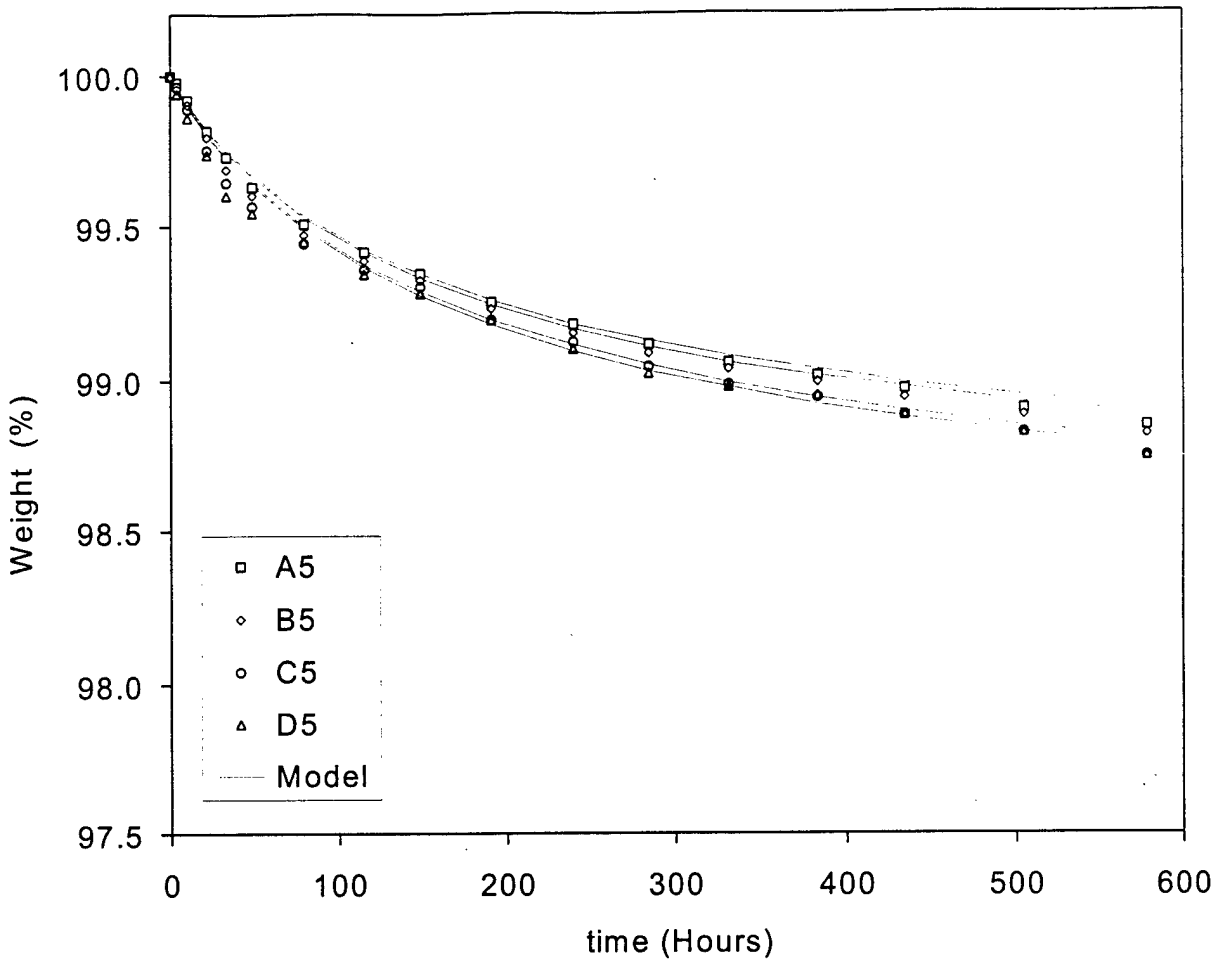

Figure 8(a) Data vs. model prediction for various lay-up sequence (a) at 180°C (c) for A5-type specimens at 170°C, 180°C, 190°C, and 200°C, respectively.

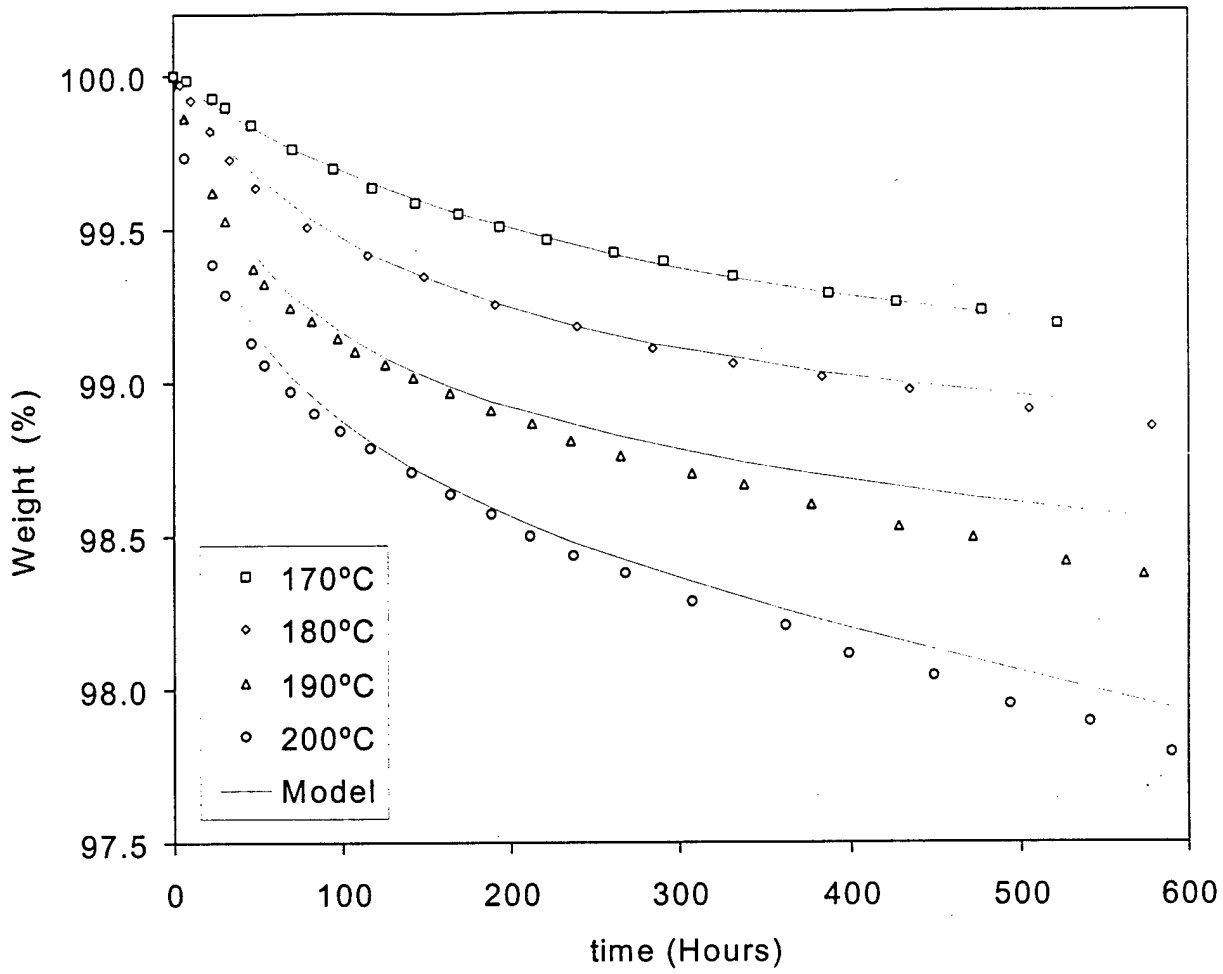

Figure 8(b) Data vs. model prediction for various lay-up sequence (a) at 180°C (b) for A5-type specimens at 170°C, 180°C, 190°C, and 200°C, respectively.

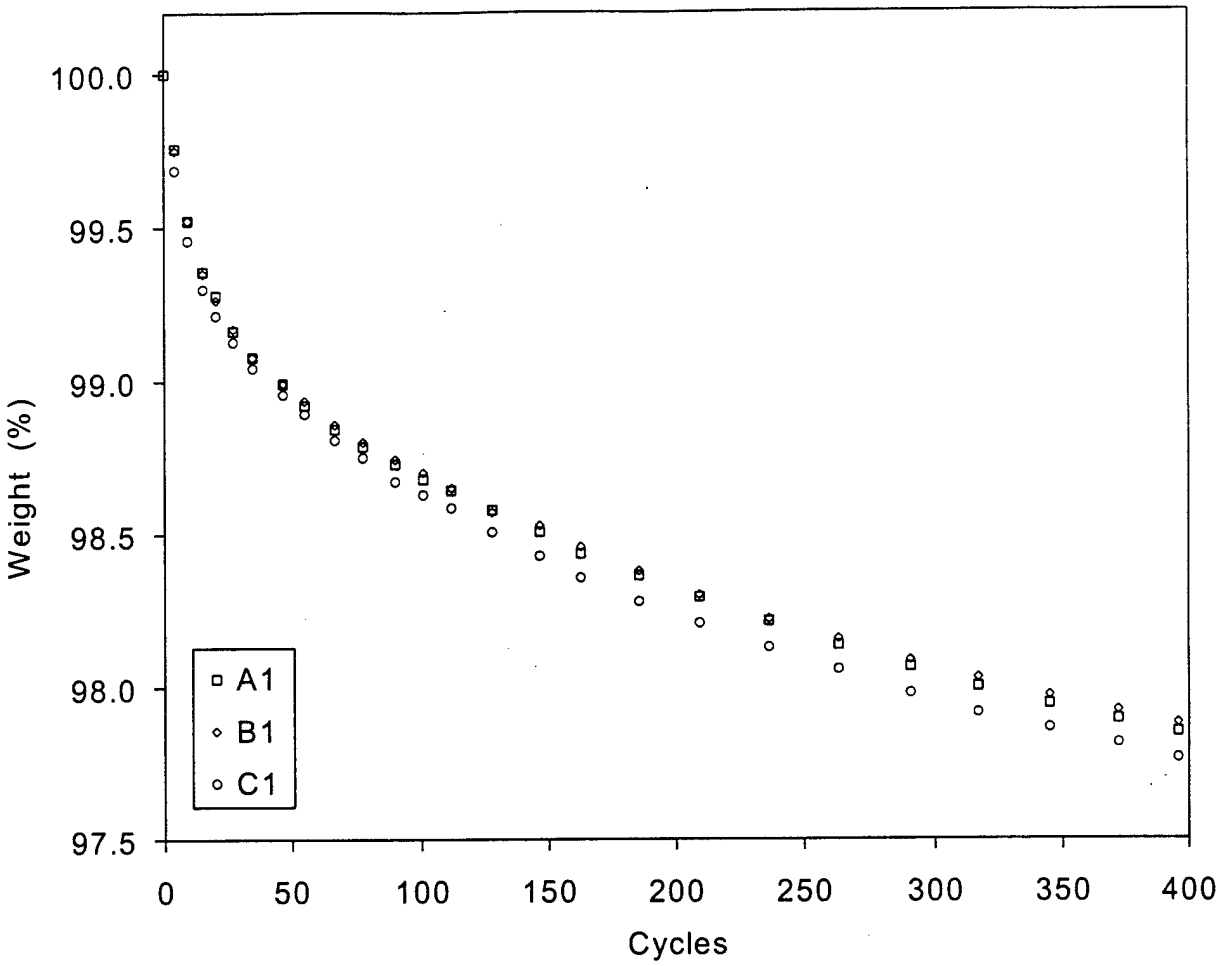

Figure 9 Effect of number of thermal cycles on sample weight change.

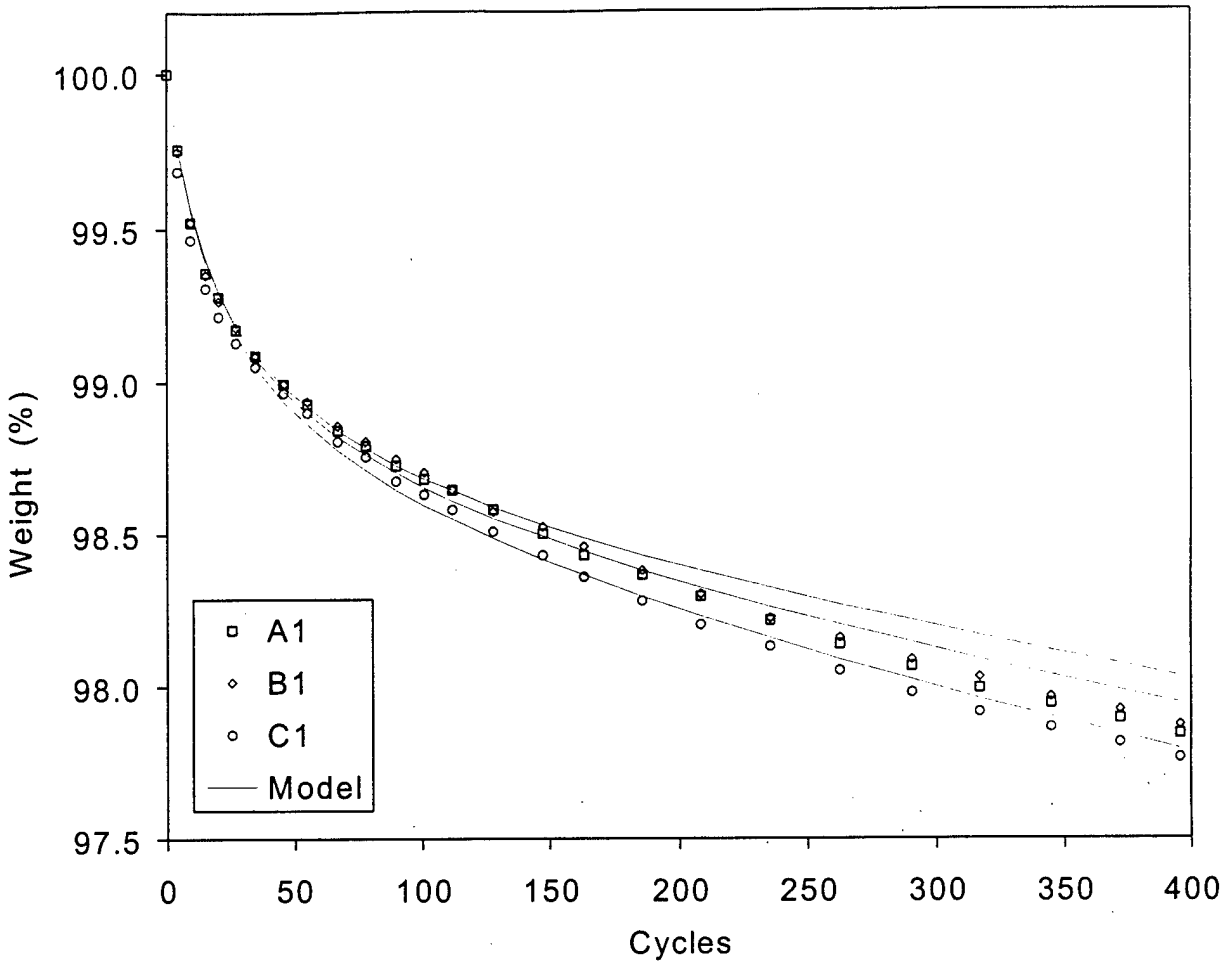

Figure 10 Experimental cycling data vs. model prediction.

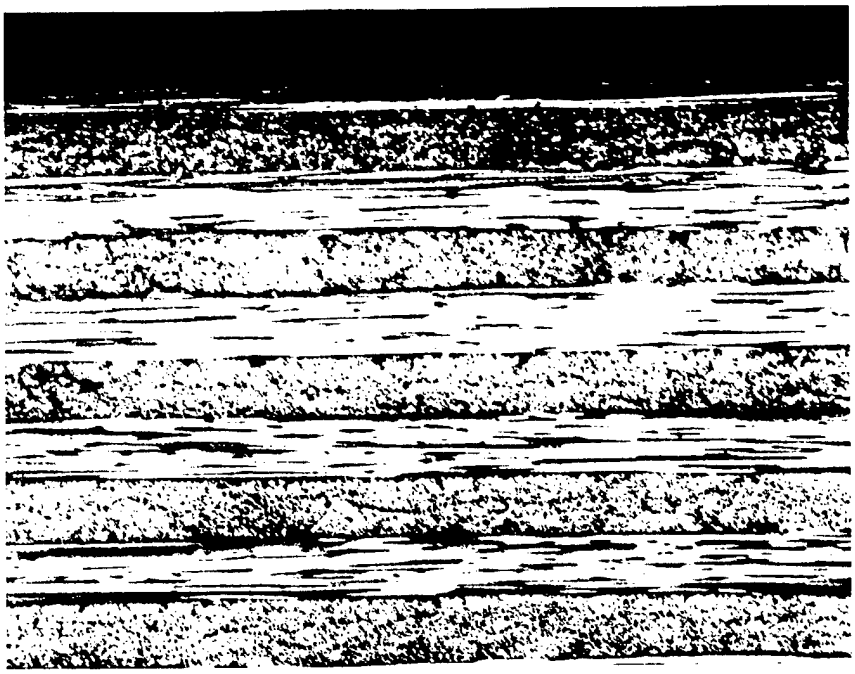

Figure 11(a)

Figure 11 Cross-section of (a) unaged specimen (b) aged specimen due to thermal cycles. Magnification = 20X.

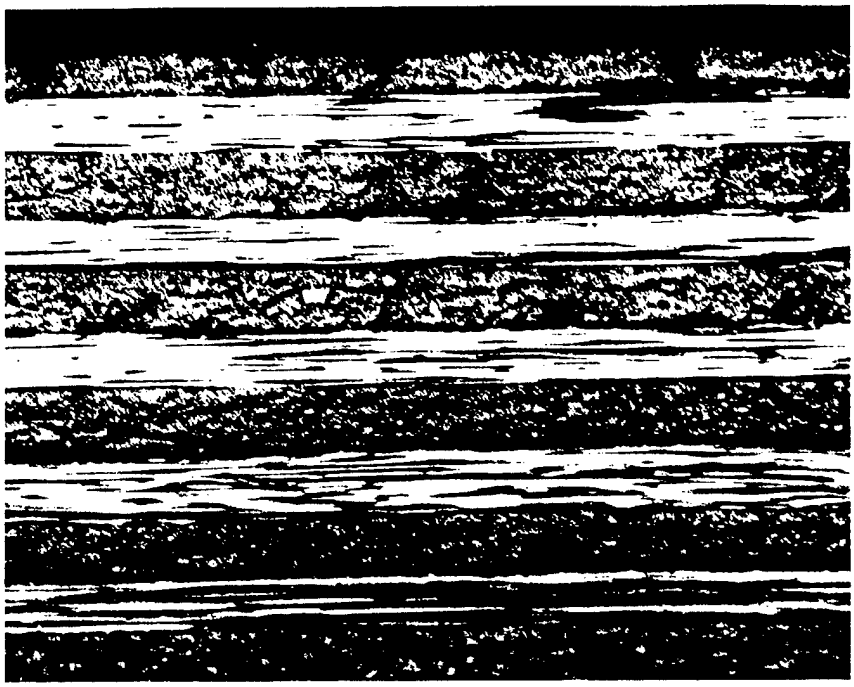

Figure 11(b)

Figure 11 Cross-section of (a) unaged specimen (b) aged specimen due to thermal cycles. Magnification = 20X.